Journal Pre-proof

Design, synthesis, and evaluation of “dual-site”-binding diarylpyrimidines targeting both NNIBP and the NNRTI adjacent site of the HIV-1 reverse transcriptase

Da Feng, Xiaofang Zuo, Lanlan Jing, Chin-Ho Chen, Fisayo A. Olotu, Hao Lin, Mahmoud Soliman, Erik De Clercq, Christophe Pannecouque, Kuo-Hsiung Lee, Dongwei Kang, Xinyong Liu, Peng Zhan

PII: S0223-5234(20)31035-7

DOI: https://doi.org/10.1016/j.ejmech.2020.113063

Reference: EJMECH 113063

To appear in: *European Journal of Medicinal Chemistry*

Received Date: 3 November 2020

Revised Date: 22 November 2020

Accepted Date: 28 November 2020

Please cite this article as: D. Feng, X. Zuo, L. Jing, C.-H. Chen, F.A. Olotu, H. Lin, M. Soliman, E. De Clercq, C. Pannecouque, K.-H. Lee, D. Kang, X. Liu, P. Zhan, Design, synthesis, and evaluation of “dual-site”-binding diarylpyrimidines targeting both NNIBP and the NNRTI adjacent site of the HIV-1 reverse transcriptase, *European Journal of Medicinal Chemistry*, https://doi.org/10.1016/j.ejmech.2020.113063.

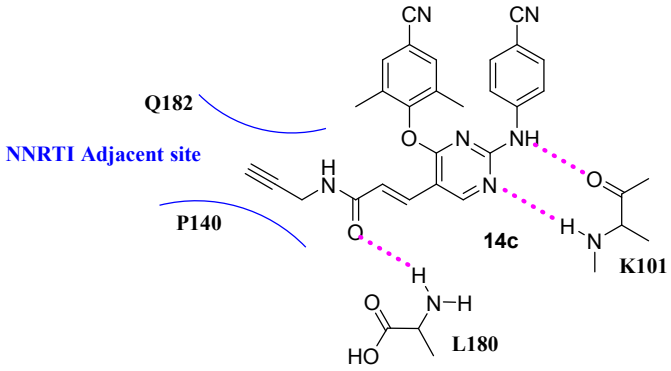

EC_{50} =

5.20 ± 1.50 nM (IIIB)

113 ± 33.4 nM (L100I)

10.4 ± 0.600 nM (K103N)

61.8 ± 13.2nM (Y181C)

64.5 ± 15.6 nM (Y188L)

10.6 ± 3.00 nM (E138K)

402 ± 313 nM (F227L + V106A)

1291± 290 nM (RES056)

Design, synthesis, and evaluation of "dual-site"-binding diarylpyrimidines targeting both NNIBP and the NNRTI adjacent site of the HIV-1 reverse transcriptase

Da Feng,[†#] Xiaofang Zuo,[†#] Lanlan Jing,[†] Chin-Ho Chen,[ζ] Fisayo A. Olotu,[Ψ] Hao Lin,[†] Mahmoud Soliman,[Ψ] Erik De Clercq,[§] Christophe Pannecouque,[§] Kuo-Hsiung Lee,[ζ] Dongwei Kang,[†,&,*] Xinyong Liu,[†,&,*] Peng Zhan[†,&,*]

[†] *Department of Medicinal Chemistry, Key Laboratory of Chemical Biology (Ministry of Education), School of Pharmaceutical Sciences, Cheeloo College of Medicine, Shandong University, 44 West Culture Road, 250012 Jinan, Shandong, PR China*

[ζ] *Natural Products Research Laboratories, Eshelman School of Pharmacy, University of North Carolina, Chapel Hill, North Carolina 27599, United States*

[Ψ] *Molecular Bio-computation and Drug Design Laboratory, School of Health Sciences, University of KwaZulu-Natal, Westville Campus, Durban 4001, South Africa.*

[§] *Rega Institute for Medical Research, Laboratory of Virology and Chemotherapy, K.U. Leuven, Herestraat 49 Postbus 1043 (09.A097), B-3000 Leuven, Belgium.*

[&] *China-Belgium Collaborative Research Center for Innovative Antiviral Drugs of Shandong Province, 44 West Culture Road, 250012 Jinan, Shandong, PR China*

Abstract:

Inspired by our previous efforts to improve the drug-resistance profiles of HIV-1 non-nucleoside reverse transcriptase inhibitors (NNRTIs), a novel series of "dual-site" binding diarylpyrimidine (DAPY) derivatives targeting both the NNRTI adjacent site and NNRTIs binding pocket (NNIBP) were designed, synthesized, and evaluated for their anti-HIV potency in TZM-bl and MT-4 cells. Eight compounds exhibited moderate to excellent potencies in inhibiting wild-type (WT) HIV-1 replication with EC_{50} values ranging from 2.45 nM to 5.36 nM, and **14c** (EC_{50} = 2.45 nM) proved to be the most promising inhibitor. Of note, **14c** exhibited potent activity against the single mutant strain E138K (EC_{50} = 10.6 nM), being comparable with ETR (EC_{50} = 9.80 nM) and 3.5-fold more potent than that of compound **7** (EC_{50} = 37.3 nM). Moreover, **14c** acted as a classical NNRTI with high affinity for WT HIV-1 RT (IC_{50} = 0.0589 μM). The detailed structure-activity relationships (SARs) of the representative compounds were also determined, and further supported by molecular dynamics simulation. Overall, we envision that the "dual-site"-binding NNRTIs have significant prospects and pave the way for the next round of rational design of potent anti-HIV-1 agents.

Keywords: HIV-1; "Dual-site" binding NNRTI; NNIBP; NNRTI adjacent site; Drug design; Molecular dynamics simulation

1. Introduction

Reverse transcriptase (RT) is an important enzyme in the life cycle of HIV-1, the etiologic agent of acquired immunodeficiency syndrome (AIDS). Non-nucleoside RT inhibitors (NNRTIs) as promising anti-HIV drugs are widely used in highly active antiretroviral therapy (HAART) regimens on account of their excellent antiviral potency, low toxicity, high specificity, and favorable pharmacokinetic properties [1-3]. Up till 2020, there were sixNNRTIs approved by the US FDA (**Fig. 1**) [4]. However, drug resistance to the first generation of NNRTIs including nevirapine (**1**, NVP), delavirdine (**2**, DLV), and efavirenz (**3**, EFV) emerged rapidly because of the replication infinity and genetic variability of HIV-1 (**Fig. 1**). Although etravirine (**4**, ETR) and rilpivirine (**5**, RPV), the second generation of NNRTIs approved by the US FDA in 2008 and 2011, respectively, displayed significantly improved drug-resistance profiles, low solubility and poor oral bioavailability limited their clinical application [5-10]. Moreover, the E138K viral strain with a major mutation conferring resistance to ETR and RPV [11, 12]. In 2017, Elsulfavirine was approved by Russia as a prodrug. It exhibited antiviral potency with an EC50 value of 1.2 nM against the WT HIV RT [7]. In 2018, doravirine (**6**, DOR) was approved by the FDA, due to its excellent activity towards the K103N and Y181C strains. However, it still exhibited inferior antiviral activity against the V106A and F227L strains [13, 14]. Therefore, novel

NNRTI drugs with improved potency against resistance-associated variants are highly needed.

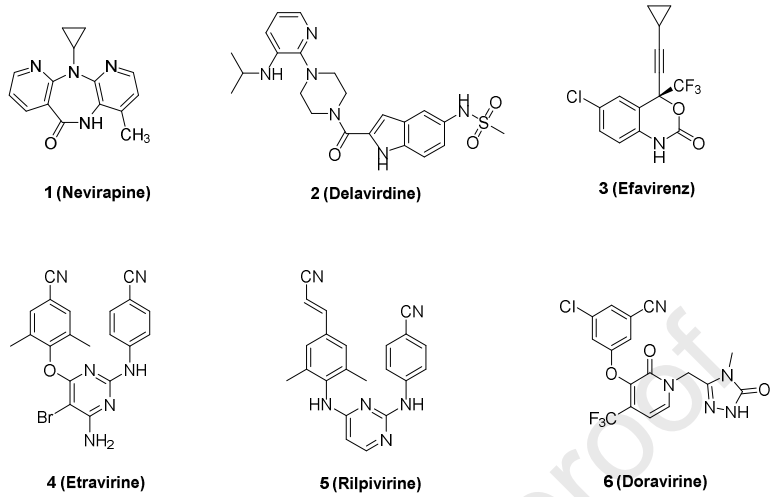

Figure 1. Structures of NNRTIs approved by the US FDA

Recently, three underexploited sites named as the "NNRTI adjacent" binding site (PDB code: 4KFB), the Knuckles site (PDB code: 4IG3), and the incoming nucleotide binding site (PDB code: 4ICL), which provided novel druggable target sites, were reported by X-ray crystallography-based fragment screening (**Fig. 2**). Among them, the NNRTI adjacent site, formed by T139 (p51), P140 (p51), T165, L168, K172, and I180, is located at the p66/p51 interface in the palm subdomain and orients towards the catalytic site with a distance of 14.46 angstroms to the NNRTI binding pocket (NNIBP). The ligand, with high electron density, showed ligand efficiency of 0.34 kcal/mol owing to the formation of hydrogen-bonding interactions with I180 and Q182 and hydrophobic forces with P140 and I180 [15-17]. To our delight, the residues P140, I180, and Q182 involved in critical interactions are highly conserved, indicating that the NNRTI adjacent site is a prospective site for the design of novel DAPY derivatives, in which we have already made some progress [11].

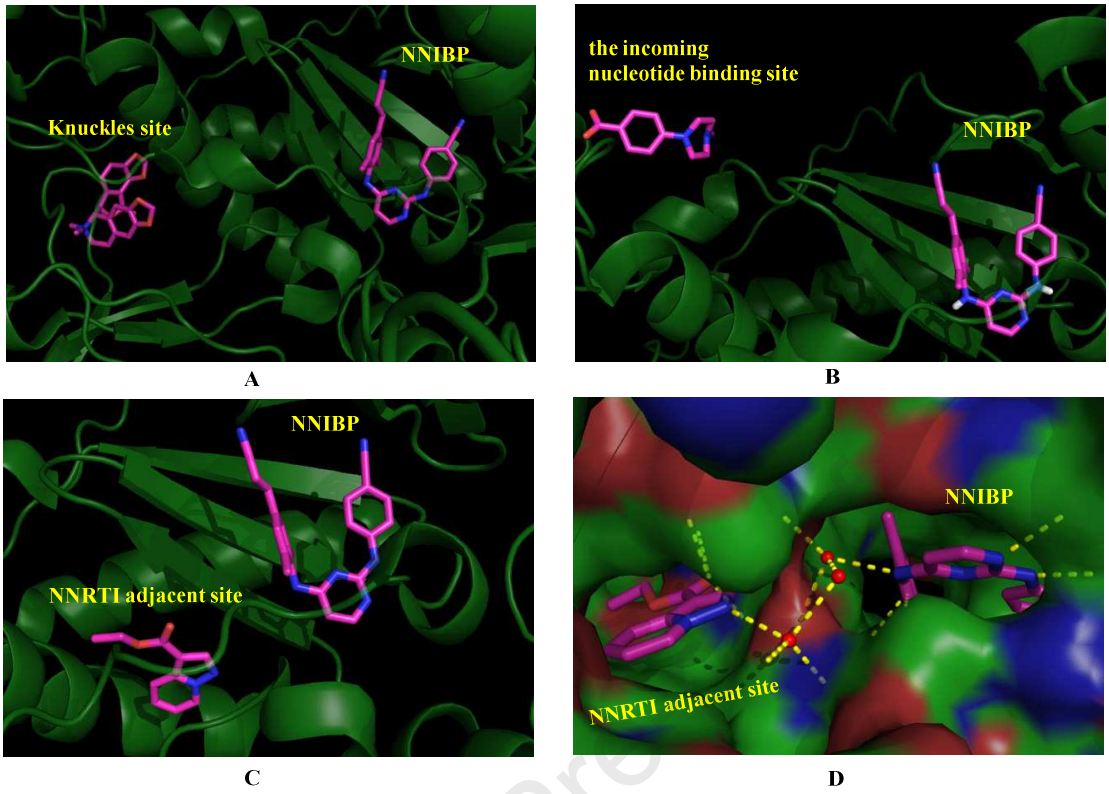

Figure 2. Novel HIV-1 RT binding sites with bound fragments: (A) near the Knuckles site (PDB Code: 4IG3); (B) at the incoming nucleotide binding site (PDB Code: 4ICL); (C, D) at the NNRTI adjacent site (PDB Code: 4KFB).

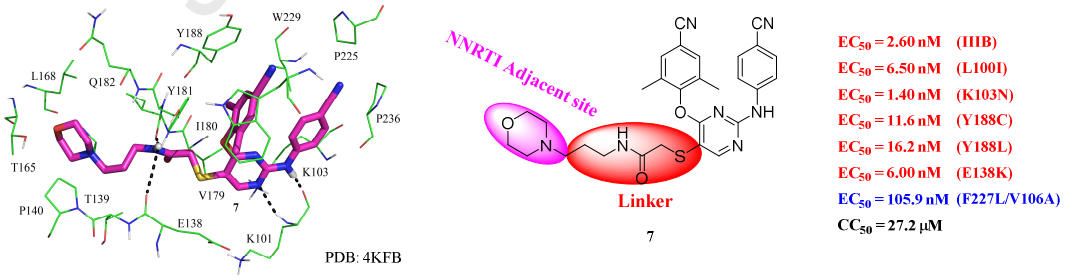

Figure 3. The binding mode and anti-HIV-1 activities of compound **7**.

Our previous studies have discovered a series of novel dual-site derivatives demonstrating favorable anti-HIV activities [17]. In particular, compound **7** showed more potent antiviral activity against WT and the single mutant strains (L100I,

K103N, Y181C, Y188L, and E138K) of HIV-1 than ETR (**Fig. 3**). Molecular modeling analysis demonstrated that compound **7** adopted a horseshoe-like conformation in the NNIBP, which was similar to that of RPV, and maintained the key double hydrogen bond with the backbone of K101 residue. In addition, NH atoms of the amide of compound **7** can form double hydrogen bonds with E138 and I180. However, compound **7** only formed a hydrogen bond with one of the conserved amino acids, namely I180. And this compound did not go deep into the bottom of adjacent sites. In addition, compound **7** showed slight efficacy against HIV-1 Y188L, E138K, and the double-mutant strains RES056. Therefore, given the results obtained from previous explorations, it is still worth further exploring the specific modification to target conserved amino acids, as well as the length and type of the linker [18].

In order to explore the structure-activity relationship (SAR) of the dual-site NNRTIs and improve the drug resistance, we preserved the privileged skeleton of the lead compound ETR. At the same time, multiple hydrogen bond donors or acceptors, such as sulfonyl amides and amide groups, were introduced into the adjacent sites of NNRTI to form hydrogen bonds with the conserved amino acid Q182. Finally, a *trans*-double bond with spatial orientation advantage was introduced to make sure the substituent stretching into the NNRTI adjacent site accurately (**Fig**. **4**). Herein, a series of novel DAPY derivatives were synthesized and evaluated, and the RT inhibition assay, molecular modeling, and physicochemical properties were also discussed.

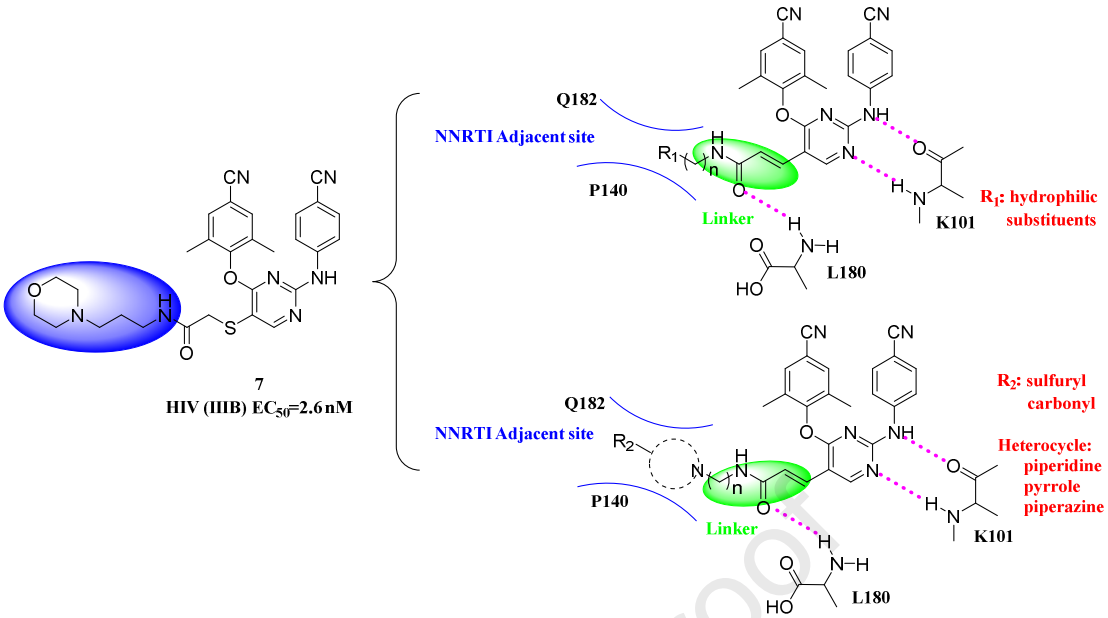

Figure 4. The design of new compounds targeting the NNIBP and the NNRTI adjacent site.

2. Results and discussion

2.1. Chemistry

The synthetic routes of the newly designed compounds are depicted in **Scheme 1**. The commercially available material 2,4-dichloropyrimidine (**8**) was transformed into intermediate **9** by reaction with 3,5-dimethyl-4-hydroxybenzonitrile. Then **10** was afforded by the Buchwald-Hartwig reaction of **9** and 4-aminobenzonitrile. Subsequently, the key intermediate **11** was obtained in the presence of *N*-iodosuccinimide (NIS) and trifluoroacetic acid (TFA) *via* the electrophilic substitution. Next, treatment of **11** with ethyl acrylate gave intermediate **12** by means of Heck reaction and **13** was obtained by hydrolyzing **12** with lithium hydroxide. The target compounds **14a–i** and important intermediates **15a-f** were obtained by condensation of **13** with the corresponding amine. The Boc group on **15a-f** was removed with TFA at room temperature to afford intermediate **16**. Finally, the target compounds **17–l** were obtained through acylation. All newly synthesized compounds

were confirmed by their physicochemical data as well as MS and ^{1}H and ^{13}C NMR spectral means.

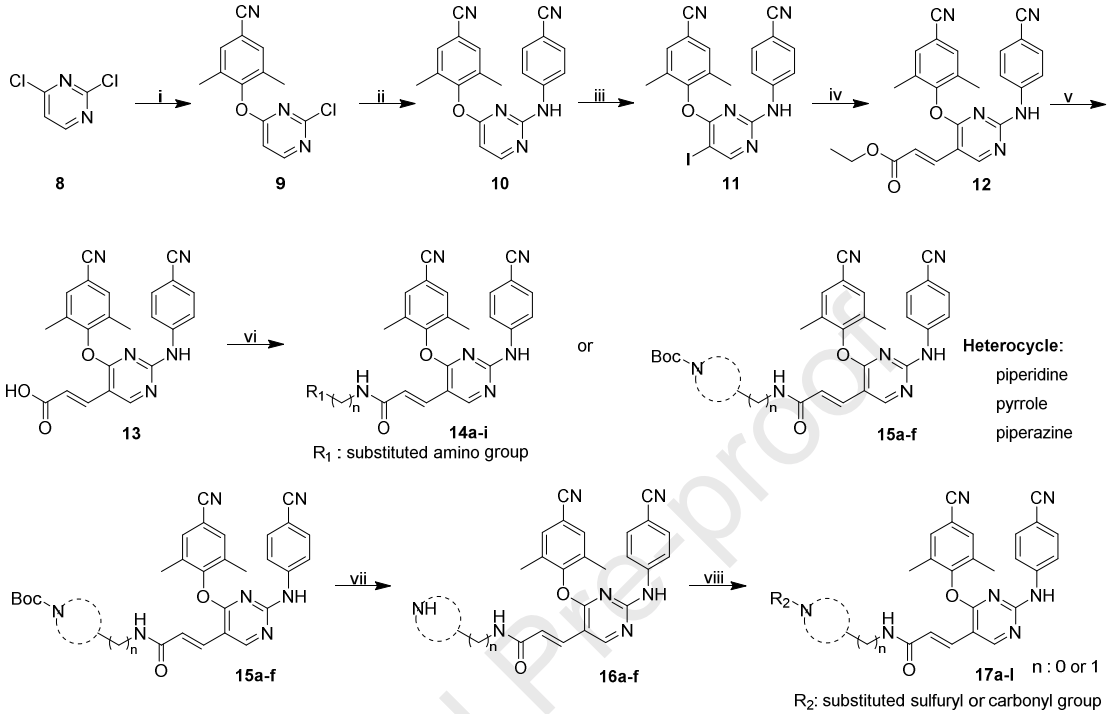

Scheme 1. Reagents and conditions: (i) 3,5-dimethyl-4-hydroxybenzonitrile, K_2CO_3, DMF, r.t.; (ii) Xantphos, $Pd(AcO)_2$, Cs_2CO_3, 1,4-dioxane, N_2, 80 °C; (iii) NIS, TFA, CH_3CN, r.t.; (iv) ethylacrylate, $Pd(AcO)_2$, PPh_3, CH_3COONa, DMF, N_2, 110 °C; (v) THF/H_2O (1:1), LiOH; (vi) amino-containing intermediates, HATU, DIEA, DMF, 0 °C to r.t.; (vii) TFA, DCM, r.t.; (viii) acyl chloride or sulfonyl chloride, Et_3N, DCM, 0 °C to r.t.

2.2. Anti-HIV activity evaluation

The target compounds were evaluated against the wild-type (WT) HIV-1 (NL4-3) replication in the TZM-bl cell line. NVP, EFV, ETR, and AZT were selected as reference drugs, compound **7** was selected as control. The values of EC_{50} (anti-HIV potency), CC_{50} (cytotoxicity), and SI (selectivity index, CC_{50}/EC_{50} ratio) of the target

compounds are summarized in **Tables 1** and **2**.

As illustrated in **Tables 1** and **2**, all of the novel compounds exhibited moderate to excellent nanomolar or micromolar antiviral activities against WT HIV-1, with EC_{50} values ranging from 2.45–81.28 nM, except for **17c**, **17d**, and **17h**. Among them, compounds **14a**–**f**, **14h**, and **17l** proved to be single-digit nanomolar inhibitors with EC_{50} values of 2.45–5.36 nM. Compound **14c** (EC_{50} = 2.45 nM) was the most potent inhibitor, being equipotent to that of ETR (EC_{50} = 1.45 nM) and about 1.5-fold more potent than the lead **7** (EC_{50} = 3.77 nM). Moreover, **14c** demonstrated lower cytotoxicity (CC_{50} > 222 nM).

To further verify the activity of the potent compounds **14c**–**f**, **14h**, and **17l**, they were further evaluated for their activities in cultured MT-4 cells infected with the WT HIV-1 strain (IIIB) as well as a panel of NNRTIs-associated single and double mutant strains, including L100I, K103N, Y181C, Y188L, E138K, F227L + V106A, and K103N + Y181C (RES056). NVP, EFV, ETR, and AZT were selected as reference drugs, compound **7** was selected as control, the results are displayed in **Table 3**.

As their activity in TZM-bl cell line, all of the selected derivatives exhibited potent activity (EC_{50} = 5.20–27.1 nM) against HIV-1 IIIB in MT-4 cells. Among them, compound **14c** exhibited extremely high potency against WT HIV-1 (EC_{50} = 5.20 nM), which was about 16.2- and 3.5-fold more potent than NVP (EC_{50} = 84.0 nM) and AZT (EC_{50} = 18.3 nM). In addition, **14c** exhibited lower cytotoxicity and higher SI (CC_{50} = 140 μM, SI = 26934) towards HIV-1 IIIB. None of them showed activity against HIV-2 ROD in MT-4 cells.

Their activity against mutant HIV-1 strains demonstrated that these compounds exhibit good activity against single mutant strains K103N, Y188L and E138K (**Table 4**). **14c** and **17l** showed higher potency against the K103N mutant strain with EC_{50} values of 10.4 and 8.70 nM, about 4.5- and 3.8-fold lower than those of ETV and compound **7** (EC_{50} = 2.30 and 2.20 nM, respectively). In the case of Y188L, **14c** (EC_{50} = 64.5 nM) and **14f** (EC_{50} = 90.6 nM) provided satisfactory potency; they were about 64- and 1.6-fold more potent than EFV (EC_{50} = 148 nM). Moreover, **14c** inhibited the most prevalent single mutant E138K with extremely high activity (EC_{50} = 10.6 nM), being equipotent to ETR (EC_{50} = 9.80 nM), which was about 3.5-fold more potent than compound **7** (EC_{50} = 37.3 nM). Although most of the derivatives showed promising activities toward HIV-1 single mutant strains K103N and E138K, their potencies against RES056 were inferior to that of the reference drugs (**7**, AZT, EFV, and ETR).

Table 1. Anti-HIV-1 activity and cytotoxicity of compounds **12** and **14a–i**.

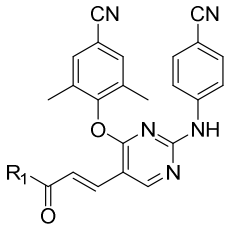

12 and **14a-i**

Compds.	R_1	EC_{50} (nM) [a] NL4-3	CC_{50} (nM) [b]	SI (NL4-3) [c]
12		18.7 ± 3.87	**>** 227	>12.0

14a		5.36 ± 1.66	**>** 243	>45.0
14b		5.10 ± 1.22	**>** 221	>44.0
14c	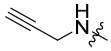	2.45 ± 0.710	**>** 222	>91.0
14d	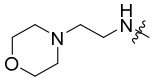	3.44 ± 1.18	**>** 190	>56.0
14e	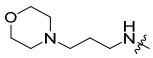	3.53 ± 0.950	**>** 186	>53.0
14f	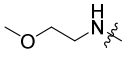	4.48 ± 1.19	**>** 213	>48.0
14g	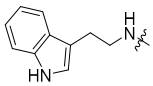	81.3 ± 21.7	**>** 180	>2.00
14h	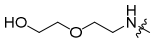	4.81 ± 1.48	**>** 200	>42.0
14i		20.0 ± 5.41	**>** 208	>10.0
7	--	3.77 ± 1.38	**>** 179	>48.0
NVP	--	281 ± 38.7	>15000	>53.0
EFV	--	5.20 ± 0.900	>6300	>1212
ETR	--	1.45 ± 0.500	**>** 229	>158
AZT	--	7.50 ± 1.80	>6300	>1004

[a]EC_{50}: concentration of compound that causes 50% inhibition of viral infection and determined in at least triplicate against HIV-1 virus in TZM-bl cell lines. NL4-3 is wild-type HIV-1 viral strain. [b]CC_{50}: concentration that is cytopathic to 50% of the cells. The highest concentration of the tested compounds was 100 ng/mL. [c]SI: selectivity index, the ratio of CC_{50}/EC_{50}.

Table 2. Anti-HIV-1 activity and cytotoxicity of compounds **17a–l**.

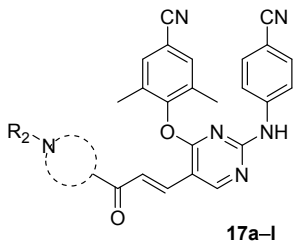

17a–l

Compds.	**The group in the**	**R_2**	**EC_{50} (nM) [a]**	**CC_{50} (nM) [b]**	**SI (NL4-3) [c]**

	dotted circle		NL4-3		
17a	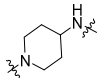		14.2 ± 4.90	**>** 175	>12.0
17b	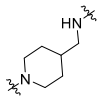		12.8 ± 3.24	**>** 171	>13.0
17c	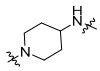		**>** 160	**>** 160	>1.00
17d	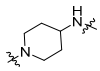		**>** 170	**>** 170	>1.00
17e	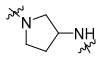		14.7 ± 3.23	**>** 179	>12.0
17f	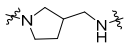		13.6 ± 4.37	**>** 175	>13.0
17g			13.8 ± 5.20	**>** 179	>13.0
17h			**>** 164	**>** 164	>1.00
17i			13.7 ± 2.78	**>** 174	>13.0
17j			49.9 ± 9.78	**>** 192	>4.00
17k			49.3 ± 14.38	**>** 197	>4.00
17l	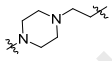		4.16 ± 1.46	**>** 166	>40.0
7	--	--	3.77 ± 1.38	**>** 179	>48.0
NVP	--	--	281 ± 38.7	>15000	>53.0
EFV	--	--	5.20 ± 0.900	>6300	>1212
ETR	--	--	1.45 ± 0.50	**>** 230	>158
AZT	--	--	7.50 ± 1.80	>6300	>1004

[a]EC_{50}: concentration of compound that causes 50% inhibition of viral infection and determined in at least triplicate against HIV-1 virus in TZM-bl cell lines. [b]CC_{50}: concentration that is cytopathic to 50% of the cells. The highest concentration of the tested compounds was 100 ng/mL. [c]SI: selectivity index, the ratio of CC_{50}/EC_{50}.

Table 3. Anti-HIV activity and cytotoxicity of **14c–f**, **14h** and **17l**.

Compds.	EC_{50} (nM)[a]	CC_{50} (μM)[b]	SI (IIIB)[c]

	IIIB	ROD		
14c	5.20 ± 1.50	> 140538	141 ± 37.7	26934
14d	8.50 ±3.10	> 22383	22.4 ± 7.30	2630
14e	10.5 ± 2.00	> 23027	23.0 ± 10.4	2199
14f	7.80 ± 2.60	> 266797	> 267	> 34341
14h	27.1 ± 10.0	> 61760	61.8 ± 63.4	2278
17l	6.10 ± 1.30	> 5859	5.90 ± 0.800	955
7	3.70 ± 1.40	> 24027	24.0	6535
NVP	84.0 ± 10.7	--	> 9.50	> 113
AZT	18.3 ± 4.2	--	> 7.50	> 410
EFV	2.50 ± 0.800	--	> 6.30	> 2572
ETR	3.00 ± 0.600	--	> 4.60	> 1546

[a]EC_{50}: concentration of compound required to achieve 50% protection of MT-4 cell cultures against HIV-1-induced cytopathic effect, as determined by the MTT method. [b]CC_{50}: concentration required to reduce the viability of mock-infected cell cultures by 50%, as determined by the MTT method. [c]SI: the ratio of CC_{50}/EC_{50}.

Table 4. Anti-HIV activity and cytotoxicity of **14c–f**, **14h** and **17l**.

Compds.	EC_{50} (nM)[a]						
	L100I	**K103N**	**Y181C**	**Y188L**	**E138K**	**F227L/V106A**	**RES056**
14c	113 ± 33.4	10.4 ± 0.600	61.8 ± 13.2	64.5 ± 15.6	10.6 ± 3.00	402 ± 313	1291± 290
14d	263 ± 66.1	18.5 ± 3.60	108 ± 16.2	123 ± 21.0	21.8 ± 4.60	462 ± 87.5	1746 ± 599
14e	254 ± 79.6	22.0 ± 0.700	124 ± 45.7	212 ± 25.6	22.6 ± 5.00	443 ± 415	1209 ± 463
14f	166 ± 50.7	13.7 ± 3.00	98.0 ± 76.5	90.6 ± 17.0	16.5 ± 5.70	343 ± 53.7	1492 ± 563
14h	227 ± 42.7	50.3 ± 14.1	197 ± 34.2	146 ± 3.80	47.1 ± 8.00	318 ± 89.0	1052 ± 372
17l	78.6 ± 31.4	8.70 ± 3.10	48.6 ± 13.1	101 ±24.3	20.9 ± 0.800	251 ± 91.7	808 ± 180
7	16.3 ± 2.80	2.20 ± 0.500	19.1 ± 4.60	38.7 ± 6.10	37.3 ± 9.60	182 ± 121	332 ± 82.0
NVP	373 ± 154	1470 ± 458	2325 ± 1074	3388 ± 1331	72.8 ± 20.6	2730 ± 1258	6748 ± 2323
AZT	7.00 ± 2.60	12.6 ± 3.40	8.70 ± 1.70	9.90 ± 7.80	14.50 ± 2.70	4.70 ± 1.70	20.1 ± 4.70
EFV	30.8 ± 18.4	63.7 ± 14.6	5.20 ± 1.70	148 ± 40.8	5.70 ± 1.20	169 ± 63.9	273 ±153
ETR	10.2 ± 10.3	2.30 ± 0.400	14.0 ± 2.60	15.5 ± 6.80	9.80 ± 3.80	8.20 ± 2.20	60.2 ± 24.7

[a]EC_{50}: concentration of compound required to achieve 50% protection of MT-4 cell cultures against the HIV-1-induced cytopathic effect, as determined by the MTT assay.

On the basis of the activity against WT HIV-1 strain, the preliminary SARs could be summarized according to the length of the chain, size of the ring, and different terminal substitution groups. By comparing **14d** (EC_{50} = 3.44 nM), **14e** (EC_{50} = 3.53 nM) with **14i** (EC_{50} = 20.0 nM), **17a** (EC_{50} = 14.2 nM) with **17b** (EC_{50} = 12.8 nM), **17e** (EC_{50} = 14.7 nM) with **17f** (EC_{50} = 13.6 nM), **17j** (EC_{50} = 49.9 nM) with **17k** (EC_{50} = 49.3 nM), and **17l** (EC_{50} = 4.16 nM) with **17g** (EC_{50} = 13.8 nM) for their activity against WT HIV-1, we observed that the antiviral activities were not exactly related to the length of carbon chain, which only presented distinct conformations for the compounds. Comparison of the activities of **17c** (sulfone, EC_{50} >160 nM) with **17d** (carbonyl, EC_{50} > 170 nM), **17g** (sulfone, EC_{50} =13.8 nM) with **17j** (carbonyl, EC_{50} =49.9 nM), and **17h** (sulfone, EC_{50} >164 nM) with **17i** (carbonyl, EC_{50} =13.7 nM) suggested that the sulfone group has a negative impact on the antiviral activity. When we compared **17g** (EC_{50} = 13.8 nM) with their fluoro-derivatives **17h** (EC_{50} > 164 nM) and **20i** (EC_{50} = 13.7 nM), and similarly **17a** (EC_{50} = 14.2 nM) with **17c** (> 160 nM) and **17d** (>170 nM), it seemed that the fluoro-group appeared to be detrimental for their antiviral potency against WT HIV-1. Interestingly, the compounds with polar groups such as morpholine (**14d**, 3.44 nM and **14e**, 3.53 nM), methoxy (**14f**, 4.48 nM), and diglycol (**14h**, 4.81 nM), showed higher anti-HIV potency than those with less polar groups. It is remarkable that the compounds bearing smaller groups with shorter linkers (**12**, **14a-c**) displayed better inhibitory activity than those with bulky groups like indole (**14g**).

2.3. HIV-1 RT inhibition assay

To further validate the binding target, the representative compound **14c** was chosen to evaluate its ability to inhibit recombinant WT HIV-1 RT enzyme, and the result is shown in **Table 5**. As expected, **14c** showed excellent affinity to HIV-1 RT with an IC_{50} value of 0.059 μM, which was nearly 6-fold greater than that of ETV (IC_{50} = 0.350 μM), and comparable to that of **7** (IC_{50} = 0.035 μM). The results proved that the newly synthesized compounds showed high affinity to HIV-1 RT, thus acting as typical HIV-1 NNRTIs. The remarkable difference between the anti-HIV activity and RT-inhibitory potency of **14c** was considered to be the variations in the HIV-1 RT-substrate binding affinities and polymerase processivity on different nucleic acid templates [19, 20].

Table 5. Inhibitory activity against HIV-1 RT (WT).

Compds.	14c	7	ETR
IC_{50} (μM) [a]	0.059	0.035	0.350

[a] IC_{50}: inhibitory concentration of tested compounds required to inhibit biotin deoxyuridine triphosphate (biotin-dUTP) incorporation into the HIV-1 (WT) RT by 50%.

2.4. Molecular docking (MD) simulation

To better understand the activity results and investigate their SARs, the representative compounds **14c** and **17l** were analyzed by MD simulation to study their binding modes with adjacent sites of NNIBP and NNRTI in HIV-1 RT (PDB Code: 4KFB).

2.4.1. Ligand induced structural stability

As stated previously, we made a thorough comparison of the structural effects of both compounds (**14c** and **17l**) when bound at the NNIBP. We investigated the

structural dynamics of the proteins by estimating the Cα root mean square deviation (RMSD), fluctuation (RMSF), and structural compactness by radius of gyration (RoG). RMSD analysis was intended to investigate the dynamics and motions of constituent C-α atoms, RMSF; per-residue fluctuation and RoG compactness (**Table 6**).

Table 6: Estimated values from whole structural analysis and analysis of binding site regions

Systems	Whole Structural Analysis		Binding Site Regions	
	14c → NNIPB	**17l → NNIBP**	**14c → NNIPB**	**17l → NNIBP**
RMSD (Å)	4.6 ± 0.8	4.1 ± 1.2	2.2 ± 0.2	2.1 ± 0.2
RMSF (Å)	2.4 ± 0.8	2.8 ± 1.0	1.6 ± 0.2	1.9 ± 0.4
RoG (Å)	35.4 ± 0.7	35.7 ± 0.7	9.9 ± 0.1	9.6 ± 0.1

Based on our findings, the protein was more structurally stable in the presence of **17l** with a higher RMSD relative to **14c** bound system (**Fig. 5**). Estimated mean values are presented in **Table 6** to the effects of **14c** as deduced from the RMSF calculations.

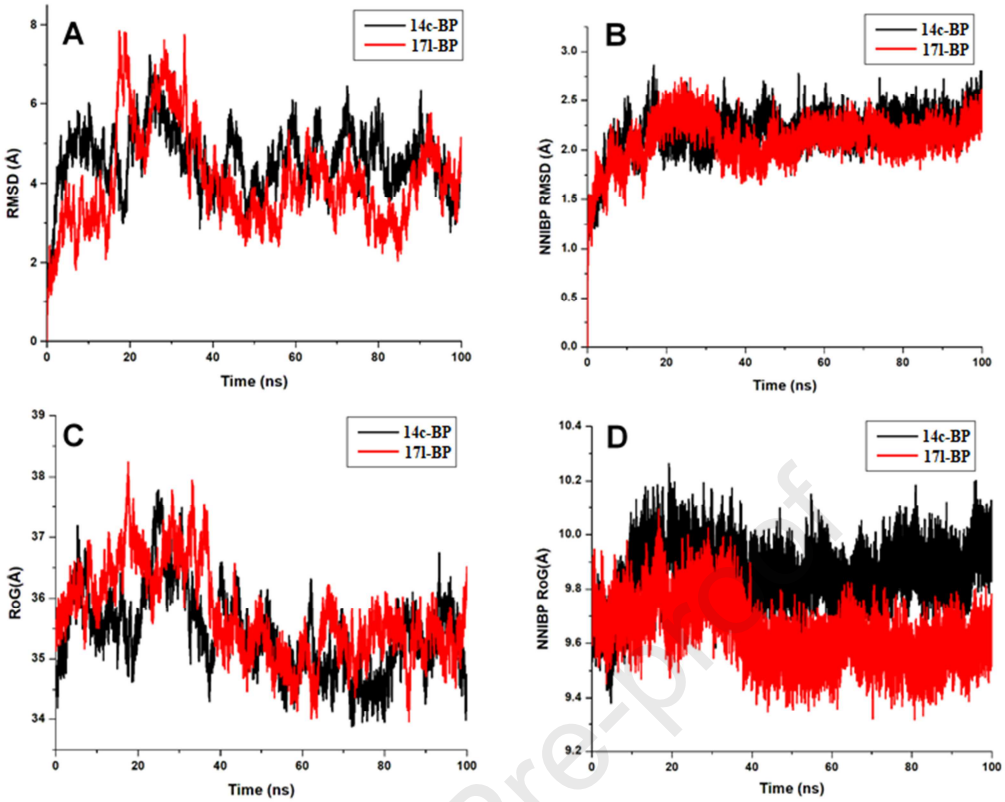

Figure 5. RMSD and RoG analyses for whole protein and NNIBP region in the presence of **14c** (black) and **17l** (red). (A). RMSD analysis of structural stability for entire structure; (B). NNIBP region; (C). RoG analyses for entire protein complex; (D). RoG analysis of NNIBP compactness.

This could imply that the protein maintained a degree of conformational rigidity in the presence of **14c**. Alternatively, variations in structural compactness were observed among both proteins, as measured using the RoG metrics (**Fig. 5**). However, the NNIBP region was highly stable and compact in the presence of **17l** compared to when bound by **14c**. These differential NNIBP stabilities were determined by masking the NNIBP regions for RoG and RMSD analyses. A more compact NNIBP would favor the stable and high-affinity binding of **17l**. Estimated values are presented in **Table 6**. Also, we could suggest that the binding activity of **17l** at this region could be

more favorable than that of **14c**.

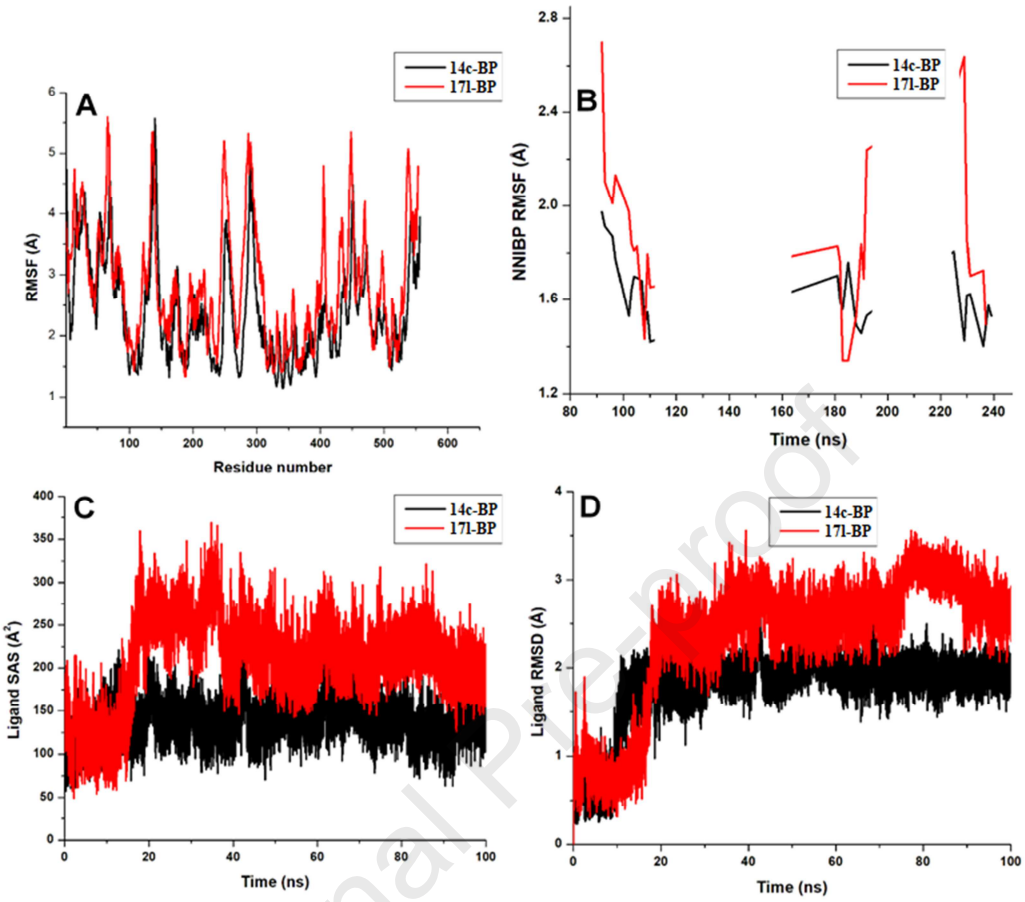

Figure 6. Analyses of per-residual fluctuation in (A). Overall protein structure; (B). NNIBP region. Ligand motions were determined in the **14c** system (black) and **17l** (red) using; (C). SASA analysis; (D). RMSD calculation.

Notably, motions of individual residues at the NNIBP region were higher in the presence of **17l**, which, presumably may be due to complementary interactions mediated by the compound. We further measured relative motions of the compounds at the NNIBP over the simulation period. From our calculations, **17l** exhibited high motions at the NNIBP region compared to **14c** with a much lower deviation (**Fig. 6**). This pattern of motion was also deduced from estimations of solvent exposure, which revealed that **17l** may be more extended into the solvent environment. This possibility

could be due to various orientations it assumed at the NNIBP to achieve optimal and stable binding. As estimated, ligand RMSD for **14c** was 1.8 Å, and 2.4 Å for **17l**. Also, ligand solvent exposure, as estimated by SASA metrics was 208.1 $Å^2$ for **17l** and 138.5 $Å^2$ for **14c** (**Table 7**).

Table 7. Estimated values from analysis of ligand motion and dynamics

Systems	14c → NNIPB	17l → NNIBP
RMSD (Å)	1.8 ± 0.4	2.4 ± 0.7
SASA ($Å^2$)	138.5 ± 0.1	208.1 ± 0.2

2.2.2. Analysis of the differential binding mechanisms of **14c** and **17l** to HIV-1 RT NNIBP

While we have analyzed differences in the structural motions and dynamics of the target protein in the presence of inhibitors, we also present herein the MM/GBSA analyses of ligand binding affinities to the NNIBP. Energy binding could also provide a yardstick for predicting the preferential binding order of the compounds for the target sites. Our calculations are shown in **Table 8**. As presented, a notably high ΔG_{bind} was associated with the binding of **17l** at the NNIBP, which is superior to the energy derived for **14c** by -21 kcal/mol. This huge energy difference is sufficient to indicate that **17l** binds HIV-RT NNIBP with a much higher affinity than **14c**. Also, electrostatic effects were raised from -2.3 (**14c**) to -43.1 kcal/mol in **17l**, while vdW energies varied by 10.6 kcal/mol. This could indicate that the high affinity binding of **17l** was greatly influenced by electrostatic and vdW energies relative to **14c**. Estimations of non-polar (ΔE_{SA}) and polar solvation (ΔG_{sol}) energies further

emphasized that the binding of **17l** was more favorable in the hydrophobic NNIBP pocket compared to**14c**.

Table 8. MM/GBSA energy calculations

Binding energies (kcal/mol)	**14c → NNIBP**	**17l → NNIBP**
ΔE_{vdw}	-58.4 ± 0.1	-69.0 ± 0.3
ΔE_{ele}	-2.3 ± 0.2	-43.1 ± 0.4
ΔE_{GB}	25.0 ± 0.2	56.8 ± 0.4
ΔE_{SA}	-7.2 ± 0.01	-8.4 ± 0.01
ΔG_{gas}	-60.8 ± 0.3	-112.2 ± 0.5
ΔG_{sol}	17.8 ± 0.2	48.3 ± 0.4
ΔG_{bind}	-42.9 ± 0.1	-63.9 ± 0.2

$\mathbf{\Delta E_{ele}}$ = electrostatic energy; $\mathbf{\Delta E_{vdW}}$ = van der Waals energy; $\mathbf{\Delta G_{bind}}$ = total binding free energy; $\mathbf{\Delta G_{sol}}$ = solvation free energy $\mathbf{\Delta G_{gas}}$ = gas phase free energy; $\mathbf{\Delta E_{GB}}$ = polar solvation energy; $\mathbf{\Delta E_{SA}}$ non-polar solvation energy.

2.4.3. Molecular details into the differential binding dynamics of **14c** and **17l** at the NNIBP region of HIV-1 RT.

We investigated the binding modes of both compounds to determine their interaction patterns over the entire simulation period. This was also important to identify NNIBP residues that contributed to ligand affinity binding and stability. The ultimate positioning and orientations of both compounds at the NNIBP is shown in **Figure 7**.

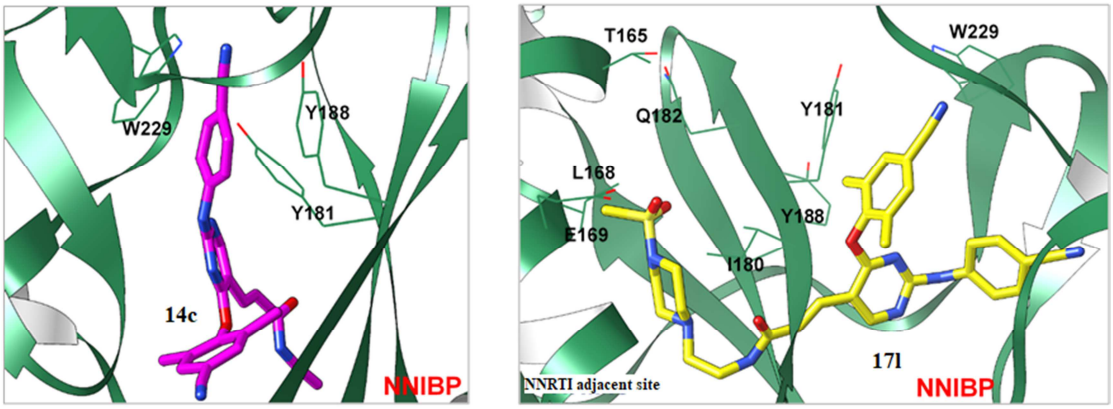

Figure 7. 3D structural representation of **14c** and **17l** positioning at the NNIBP region. The extension of **17l** methyl-sulphonyl piperazine group into the NNRTI adjacent site is shown.

Time-based analysis revealed the binding modes of **14c** at the NNIBP region which enabled it to interact with pocket residues: L100, K103, K102, L233, L234, P236, Y188, W229, Y181, V179, V106, and Y318. These interactions entailed aromatic (π), conventional and non-conventional H bonds (**Fig. 8**). Y188 played important roles stabilizing the amino benzonitrile ring while steady π–π interactions of Y181 could further stabilize the core pyrimidine ring. These ring-ring interactions are important for the stability of the ligand at the region. H bond interactions with L102, K103 and K223 could also influence the affinity of **14c** at the NNIBP.

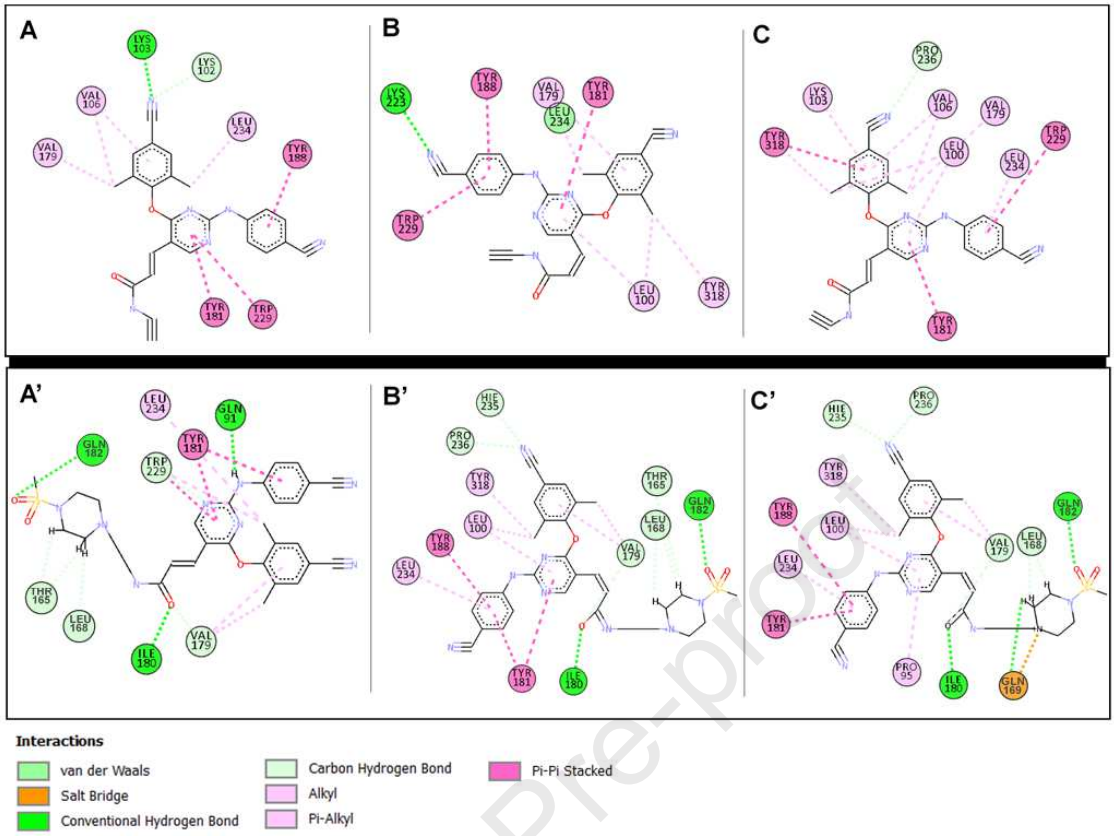

Figure 8. Analyses of complementary interactions differentially mediated by **14c** and **17l** at the NNIBP region. Interactions due to extension of the **17l** methyl-sulphonyl piperazine group were also revealed.

Similar interaction patterns, which involved Y181, Y188 and W229 were observed for the ring portions of **17l** at the NNIBP. However, additional high-affinity interactions were mediated by the methyl-sulphonyl piperazine group which extended out of the NNIBP. Also, we observed that these 'uncommon' interactions observed in **17l** mainly involved residues of the NNRTI adjacent site (**Fig. 7**).

For instance, while residues such as Y181, Y188, L234, P95, L100 stabilized the rings via aromatic (π–π, π–alkyl) interactions, with the amino-benzonitrile group of **17l**, we observed the occurrence of H bond interactions between the extended

methyl-sulphonyl piperazine group and I180, Q182, T165 and L168. Also, we observed that high number of hydrogen bonds in the **17l** complex were due to binding activities of the methyl-sulphonyl piperazine group which seemingly extended into the NNRTI adjacent site.

An important interaction that was observed at the ultimate time-frame is the salt bridge interaction between the N-H atom of the piperidine ring and *O*-atom of E169 located at the NNRTI adjacent site (**Fig. 8C**). This interaction, due to its strength could also account for the higher ΔG_{bind} estimated for **17l**. Also, the increase in H-bond, as mediated by the methyl-sulphonyl piperazine group could account for higher vdW and electrostatic energies also estimated for **17l**, as mentioned above.

3. Conclusion

In summary, to improve the drug-resistance profiles of NNRTIs, a novel series of "dual-site" binding diarylpyrimidine (DAPY) derivatives targeting both NNRTI adjacent site and NNIBP were designed, synthesized, and evaluated for their anti-HIV-1 potency. And the *trans*-double bond with spatial orientation advantage was introduced in the target compounds for the first time. Sulfonyl, acyl moieties and other privileged groups were introduced to generate additional hydrogen-bond interactions with highly conserved residue Q182 within the NNRTI adjacent site. Meanwhile, different types and lengths of linker were also investigated. The biological evaluation results demonstrated that several compounds exhibited nanomolar NL4-3 inhibitory activities in TZM-bl cells. Among them, the most

prominent compound **14c** (EC_{50} = 2.45 nM, SI > 91) showed excellent anti-HIV-1_{NL4-3} activity, which was about 1.5 times better than **7** (EC_{50} = 3.77 nM, SI > 48), and comparable to ETR (EC_{50} = 1.45 nM, SI > 158). In addition, **14c** (EC_{50} = 5.2 nM) also exhibited equivalent anti-HIV-1_{IIIB} activity to **7** (EC_{50} = 3.7 nM) and ETR (EC_{50} = 3.0 nM) in MT-4 cells. Importantly, **14c** exhibited potent activity against the single mutant strain E138K (EC_{50} = 10.6 nM), being comparable with ETR (EC_{50} = 9.80 nM) and 3.5-fold more than compound **7** (EC_{50} = 37.3 nM). Of note, the potent compound **14c** exhibited extremely low cytotoxicity and high SI values (CC_{50} = 140 μM, SI = 26934). Moreover, the HIV-1 RT inhibitory assay showed that compound **14c** (IC_{50} = 0.0589 μM) was more potent than ETR (IC_{50} = 0.35 μM), which confirmed its binding target. The dynamic simulation study showed that the *O*-atom of amide group on **17l** linker and *O*-atom on methylsulfonyl end could form hydrogen bond forces with the highly conserved amino acid residues I180 and Q182 at adjacent sites respectively, which fully verified our design hypothesis. Consequently, compounds **14c** and **17l** could serve as potential candidates for further modification to get more inhibitors targeting both NNRTI adjacent site and NNIBP.

4. Experimental Section

4.1. Chemistry

All melting points were determined on a micro melting point apparatus (RY-1G, Tianjin TianGuang Optical Instruments). ^{1}H NMR and ^{13}C NMR spectra were recorded in DMSO-d_6 on a Bruker AV-400 spectrometer with tetramethylsilane (TMS) as the internal standard. Chemical shifts are reported in δ values (ppm) from TMS,

and coupling constants are given in hertz (Hz); signals are abbreviated as s (singlet), d (doublet), t (triplet), and m (multiplet). The mass spectra were measured in AG1313A Standard LC Autosampler (Agilent). All reactions were routinely monitored by thin layer chromatography (TLC) on Silica Gel GF254 for TLC (Merck), and spots were visualized with iodine vapor or by irradiation with UV light (λ = 254 and 356 nm). Flash column chromatography was performed on columns packed with Silica Gel (Qingdao Haiyang Chemical Company). Solvents were purified and dried by standard methods and concentrated with a rotary evaporator under reduced pressure.

4-((2-Chloropyrimidin-4-yl)oxy)-3,5-dimethylbenzonitrile (9)

2,4-Dichloropyrimidine (0.10 g, 0.67 mmol), 3,5-dimethyl-4-hydroxybenzonitrile (0.12 g, 0.8 mmol), and K_2CO_3 (0.11 g, 0.8 mmol) were dissolved in *N*,*N*-dimethylformamide (DMF, 30 mL). The mixed solution was stirred for 6 h at room temperature until complete consumption of starting material as monitored by TLC. Then 50 mL of water was added and the mixture was extracted with dichloromethane (DCM, 3×10 mL), and the organic phase was washed with saturated saline (10 mL) and dried over anhydrous Na_2SO_4 to give the corresponding crude product, which was purified by silica gel chromatography to afford the target compound **9**. White powder, yield: 80%; mp: 126–128 °C; ^{1}H NMR (400 MHz, DMSO-d_6): δ 8.70 (d, J = 5.6 Hz, 1H, C_6-pyrimidine-H), 7.75 (s, 2H), 7.31 (d, J = 5.6 Hz, 2H, C_5-pyrimidine-H), 2.10 (s, 6H, $2CH_3$). ^{13}C NMR (100 MHz, DMSO-d_6): δ 169.78, 163.31, 160.45, 153.49, 134.15, 133.61, 119.62, 110.43, 108.29, 16.97. MS-ESI: *m/z* 261.10 $[M + H]^+$, $C_{13}H_{10}ClN_3O$ (calcd. 259.05).

4-((2-((4-Cyanophenyl)amino)pyrimidin-4-yl)oxy)-3,5-dimethylbenzonitrile (10)

Palladium(II) acetate (0.004 g, 0.0019 mmmol) and Xantphos (0.009 g, 0.0019 mmol) were added in 1,4-dioxane (15 mL) and stirred at room temperature for 15 min. Then, the intermediate **9** (0.1 g, 0.38 mmol) and cesium carbonate (Cs_2CO_3, 4.89 g, 0.49 mmol) were added to the above solution. The 4-aminobenzonitrile (0.16 g, 0.29 mmol) was added and 15 min later the flask was backfilled with nitrogen. The mixture was stirred at 80 °C for 6 h until complete consumption of starting material as monitored by TLC. The solution was collected by filtration under reduced pressure, and the filtrate was extracted with dichloromethane (DCM, 3×10 mL), and the organic phase was washed with saturated sodium chloride (10 mL), then dried over anhydrous Na_2SO_4 to give the corresponding crude product, which was purified by silica gel chromatography eluted with petroleum ether/EtOAc (2:1) to afford the target compound **10**. White powder, yield: 50%; mp: 126–128 °C; ^{1}H NMR (400 MHz, DMSO-d_6): δ 10.17 (s, 1H, NH), 8.51 (d, J = 5.5 Hz, 1H, C_6-pyrimidine-H), 7.79 (s, 2H), 7.57 (d, J = 8.3 Hz, 2H, C_3,C_5-Ph''-H), 7.51 (d, J = 8.4 Hz, 2H, C_2,C_6-Ph''-H), 6.72 (d, J = 5.5 Hz, 1H, C_5-pyrimidine-H), 2.12 (s, 6H, 2CH_3). ^{13}C NMR (100 MHz, DMSO-d_6): δ 169.15, 161.92, 160.33, 154.58, 145.69, 133.99, 133.97, 133.86, 120.64, 119.83, 119.46, 109.87, 103.91, 100.25, 17.07. ESI-MS: *m/z* 340.22 [M - H]$^-$, $C_{20}H_{15}N_5O$ (341.13).

4-((2-((4-Cyanophenyl)amino)-5-iodopyrimidin-4-yl)oxy)-3,5-dimethylbenzonitril e (11)

Compound **10** (0.1 g, 0.29 mmol) and *N*-iodosuccinimide (0.086g, 0.38 mmol) were

dissolved in acetonitrile (16 mL). Then, trifluoroacetic acid (88 L, 0.087 mmol) was added and stirred at room temperature for 6 h until complete consumption of starting material as monitored by TLC. After adjusting pH of the mixture to 8 with saturated sodium bicarbonate, it was filtered. The residue was dissolved in DCM (10 mL) and was purified by silica gel chromatography to afford the target compound **11**. White powder, yield: 80%; mp: 130-132 °C; ^{1}H NMR (400 MHz, DMSO-d_6): δ 10.26 (s, 1H, NH), 8.76 (s, 1H), 7.81 (s, 2H), 7.49 (d, J = 8.3 Hz, 2H), 7.44 (d, J = 8.2 Hz, 2H), 2.11 (s, 6H, $2CH_3$). ^{13}C NMR (100 MHz, DMSO-d_6): δ 166.73, 166.23, 158.86, 154.15, 144.47, 133.22, 133.03, 132.93, 119.73, 118.98, 118.78, 109.28, 103.40, 65.78, 16.15. ESI-MS: *m/z* 468.2 $[M + H]^+$, $C_{20}H_{15}IN_5O$ (467.02).

Ecethyl(*E*)-3-(4-(4-cyano-2,6-dimethylphenoxy)-2-((4-cyanophenyl)amino)pyrimidin-5-yl)acrylate (12)

Compound **11** (0.1 g, 0.21 mmol), palladium(II) acetate (0.002g, 0.007 mmol), triphenylphosphine (0.005 g, 0.019 mmol), and sodium acetate trihydrate (0.06 g, 0.44 mmol) were dissolved in DMF (30 mL), the mixture was stirred for 15 min under nitrogen. Then, ethyl acrylate (19 μL, 0.175 mmol) was added. The solution was stirred for 12 h at 110 °C until complete consumption of starting material as monitored by TLC. The solution was collected by filtration under reduced pressure, and the filtrate was extracted with dichloromethane (DCM, 3×20 mL), and the organic phase was washed with saturated sodium chloride (30 mL), then dried over anhydrous Na_2SO_4 to give the corresponding crude product, which was purified by silica gel chromatography to afford the target compound **12**. White powder, yield: 50%; mp:

148–150 °C; ^{1}H NMR (400 MHz, DMSO-d_6): δ 10.52 (s, 1H, NH), 8.96 (s, 1H, C_6-pyrimidine-H), 7.82 (s, 2H), 7.77 (d, *J* = 16.1 Hz, 1H, alkene-H), 7.48 (m, 4H), 6.76 (d, *J* = 16.1 Hz, 1H, alkene-H), 4.20 (q, *J* = 7.1 Hz, 2H, CH_2), 2.12 (s, 6H, $2CH_3$), 1.26 (t, *J* = 7.1 Hz, 3H, CH_3). ^{13}C NMR (100 MHz, DMSO-d_6): δ 166.82, 165.81, 161.89, 159.05, 153.83, 144.15, 135.80, 133.24, 133.07, 133.05, 119.65, 119.12, 118.99, 118.61, 109.31, 107.31, 103.94, 60.57, 16.20, 14.69. ESI-MS: *m/z* 438.26 [M - H]$^-$, $C_{25}H_{21}N_5O_3$ (439.16).

(*E*)-3-(4-(4-cyano-2,6-dimethylphenoxy)-2-((4-cyanophenyl)amino)pyrimidin-5-yl)acrylicacid (13)

Compound **12** (0.1g, 0.23mmol) and LiOH (0.022g, 0.92mmol) were dissolved in a mixture of 80 mL THF and 80 mL water (1:1). The mixed solution was stirred for 4 h at room temperature until complete consumption of starting material as monitored by TLC. The THF was removed under reduced pressure. After adjusting pH of the mixture to 1–2 with 1N hydrochloric acid, white solid was precipitated from the reaction solution, which was then filtered and washed with water and dried under vacuum to give **13**. White powder, ESI-MS: *m/z* 410.5 [M - H]$^-$, $C_{23}H_{17}N_5O_3$ (411.13).

*General procedure for the synthesis of target compound **17a**.*

(*E*)-3-(4-(4-cyano-2,6-dimethylphenoxy)-2-((4-cyanophenyl)amino)pyrimidin-5-yl)acrylamide (14a)

To a solution of **13** (0.15 g, 0.36 mmol) in DCM (10 mL) were added oxalyl chloride (100 μL, 1.16 mmol) and one drop of DMF. The solution was stirred at room temperature overnight. The solvent was removed under reduced pressure, and

ammonia (30 mL) was added and then reflux at 50 °C for 6 h (checked by TLC). The solution was filtered, and the residue was dissolved in DCM (10 mL). Then, ammonia (10 mL) was added again and reflux at 45 °C for 6 h. Then, the mixture was further purified by silica gel chromatography to afford target compound **14a**. White powder, yield: 50.1%; mp: 226–228 °C; ^{1}H NMR (400 MHz, DMSO-d_6): δ 10.40 (s, 1H, NH), 8.76 (s, 1H, C_6-pyrimidine-H), 7.83 (s, 2H, C_3,C_5-Ph''-H), 7.59 – 7.53 (m, 2H), 7.49 – 7.48 (m, 4H), 7.11 (s, 1H), 6.89 (d, J = 15.9 Hz, 1H, alkene-H), 2.14 (s, 6H, $2CH_3$). ^{13}C NMR (100 MHz, DMSO-d_6): δ 167.30, 165.64, 161.57, 158.43, 154.07, 144.39, 133.21, 133.10, 133.04, 131.07, 123.85, 119.72, 119.04, 118.90, 118.69, 109.22, 108.23, 103.61, 16.23. ESI-MS: *m/z* 409.26 $[M - H]^-$, $C_{23}H_{18}N_6O_2$ (410.15).

*General procedure for the synthesis of target compounds **14b–i**, **17j**, **17k** and intermediate **15a–f**.*

Compound **13** (0.1 g, 0.24 mmol) and HATU (0.11 g，0.288 mmol) were mixed in DMF (10Ml) and stirred in an ice bath for 15 min. Then, the primary amine containing polycyclic compounds (0.288 mmol) and DIEA (121 μL, 0.72 mmol) were added to the above solution slowly at 0 °C. The reaction system was stirred at room temperature for an additional 6 h (check by TLC). Then solvent was evaporated under reduced pressure, and the obtained residue was extracted with DCM (3×10 mL), and the organic phase was washed with saturated sodium chloride (10 mL), then dried over anhydrous Na_2SO_4 to give the corresponding crude product, which was purified by silica gel chromatography to afford the target compound **14b–i**, **17j**, **17k** and intermediate **15a–f**.

(*E*)-3-(4-(4-cyano-2,6-dimethylphenoxy)-2-((4-cyanophenyl)amino)pyrimidin-5-yl)-N-cyclopropylacrylamide (14b)

White powder, yield: 78.6%; mp: 254–255 °C; ^{1}H NMR (400 MHz, DMSO-d_6): δ 10.41 (s, 1H, NH), 8.75 (s, 1H, C_6-pyrimidine-H), 8.23 (d, J = 4.4 Hz, 1H, NHCO), 7.84 (s, 2H) 7.62 – 7.35 (m, 5H), 6.85 (d, J = 15.9 Hz, 1H, alkene-H), 2.84 – 2.69 (m, 1H, cyclopropane-H), 2.13 (s, 6H, $2CH_3$), 0.67 (q, J = 6.6 Hz, 2H, cyclopropane-2H), 0.50 – 0.38 (m, 2H, cyclopropane-2H). ^{13}C NMR (100 MHz, DMSO-d_6): δ 166.73, 165.62, 161.93, 158.32, 154.05, 144.39, 133.21, 133.07, 133.05, 130.39, 123.82, 119.73, 119.04, 118.88, 109.22, 108.32, 103.59, 23.04, 16.23, 6.30. ESI-MS: *m/z* 451.5 $[M + H]^+$, 468.4 $[M + NH_4]^+$, $C_{26}H_{22}N_6O_2$ (450.18).

(*E*)-3-(4-(4-cyano-2,6-dimethylphenoxy)-2-((4-cyanophenyl)amino)pyrimidin-5-yl)-N-(prop-2-yn-1-yl)acrylamide (14c)

White powder, yield: 76.6%; mp: 209–211 °C; ^{1}H NMR (400 MHz, DMSO-d_6): δ 10.43 (s, 1H, NH), 8.77 (s, 1H, C_6-pyrimidine-H), 8.65 – 8.57 (m, 1H, NHCO), 7.84 (s, 2H), 7.58 – 7.38 (m, 5H), 6.95 (d, *J* = 15.9 Hz, 1H, alkene-H), 4.00 (dd, *J* = 5.3, 2.3 Hz, 2H), 3.17 (t, *J* = 2.4 Hz, 1H, alkyne-H), 2.14 (s, 6H, $2CH_3$). ^{13}C NMR (100 MHz, DMSO-d_6): δ 173.14, 165.68, 165.44, 161.93, 160.56, 159.88, 158.45, 154.04, 144.36, 133.20, 133.09, 133.04, 131.31, 123.22, 119.71, 119.03, 118.94, 117.47, 109.24, 108.20, 103.66, 81.48, 73.67, 28.53, 16.23, 14.18. ESI-MS: *m/z* 449.4 $[M + H]^+$, 466.4 $[M + NH_4]^+$, $C_{26}H_{20}N_6O_2$ (448.16).

(*E*)-3-(4-(4-cyano-2,6-dimethylphenoxy)-2-((4-cyanophenyl)amino)pyrimidin-5-yl)-N-(2-morpholinoethyl)acrylamide (14d)

White powder, yield: 80.4%; mp: 138–140 °C; ^{1}H NMR (400 MHz, DMSO-d_6): δ 10.41 (s, 1H, NH), 8.76 (s, 1H, C_6-pyrimidine-H), 8.14 (t, *J* = 5.6 Hz, 1H, NHCO), 7.84 (s, 2H), 7.52 (s, 1H), 7.48 (m, 4H), 6.94 (d, *J* = 15.9 Hz, 1H, alkene-H), 3.64 – 3.51 (m, 4H, morpholine-4H), 3.31 – 3.29 (m, 2H), 2.38 – 2.41 (m, 6H), 2.13 (s, 6H, $2CH_3$). ^{13}C NMR (100 MHz, DMSO-d_6): δ 165.62, 161.65, 158.37, 154.08, 144.40, 133.21, 133.11, 133,04, 130.42, 123.95, 119.03, 118.89, 109.23, 108.32, 103.61, 66.61, 58.04, 53.77, 36.48, 16.25. ESI-MS: *m/z* 524.5 $[M + H]^+$, $C_{29}H_{29}N_7O_3$ (523.23).

(*E*)-3-(4-(4-cyano-2,6-dimethylphenoxy)-2-((4-cyanophenyl)amino)pyrimidin-5-yl)-N-(3-morpholinopropyl)acrylamide (14e)

White powder, yield: 81.3%; mp: 195–197 °C; ^{1}H NMR (400 MHz, DMSO-d_6): δ 10.41 (s, 1H, NH), 8.76 (s, 1H, C_6-pyrimidine-H), 8.18 (t, *J* = 5.5 Hz, 1H, NHCO), 7.84 (s, 2H), 7.65 – 7.32 (m, 5H), 6.91 (d, *J* = 15.9 Hz, 1H, alkene-H), 3.67 – 3.47 (m, 4H, morpholine-4H), 3.21 (dd, *J* = 12.6, 6.6 Hz, 2H), 2.48 – 2.21 (m, 6H), 2.13 (s, 6H, $2CH_3$), 1.71 – 1.51 (m, 2H). ^{13}C NMR (100 MHz, DMSO-d_6): δ 165.60, 165.56, 161.61, 158.35, 154.06, 144.39, 133.19, 133.09, 133.02, 130.29, 124.05, 119.70, 119.01, 118.90, 109.23, 108.35, 103.62, 66.68, 56.40, 55.36, 53.80, 26.55, 16.23. ESI-MS: *m/z* 538.5 $[M + H]^+$, $C_{30}H_{31}N_7O_3$ (537.25).

(*E*)-3-(4-(4-cyano-2,6-dimethylphenoxy)-2-((4-cyanophenyl)amino)pyrimidin-5-yl)-N-(2-methoxyethyl)acrylamide (14f)

White powder, yield: 82.6%; mp: 274–276 °C; ^{1}H NMR (400 MHz, DMSO-d_6): δ 10.34 (s, 1H, NH), 8.68 (s, 1H, C_6-pyrimidine-H), 8.20 (t, *J* = 5.3 Hz, 1H, NHCO), 7.77 (s, 2H), 7.45 (s, 1H), 7.41 (m, 4H), 6.92 (d, *J* = 15.9 Hz, 1H, alkene-H), 3.34 –

3.32 (m, 4H), 3.19 (s, 3H, CH_3), 2.07 (s, 6H, $2CH_3$). ^{13}C NMR (100 MHz, DMSO-d_6): δ 165.75, 165.62, 161.72, 158.35, 154.09, 144.41, 133.19, 133.11, 133.04, 130.49, 124.05, 119.05, 118.89, 109.19, 108.36, 103.58, 99.99, 71.16, 58.33, 39.03, 16.24. ESI-MS: *m/z* 469.4 $[M + H]^+$, $C_{26}H_{24}N_6O_3$ (468.19).

(*E*)-N-(2-(1H-indol-3-yl)ethyl)-3-(4-(4-cyano-2,6-dimethylphenoxy)-2-((4-cyanophenyl)amino)pyrimidin-5-yl)acrylamide (14g)

White powder, yield: 78.4%; mp: 225–228 °C; ^{1}H NMR (400 MHz, DMSO-d_6): δ 10.83 (s, 1H), 10.41 (s, 1H, NH), 8.77 (s, 1H, C_6-pyrimidine-H), 8.31 (t, *J* = 5.6 Hz, 1H, NHCO), 7.84 (s, 2H), 7.57 – 7.55 (m, 2H), 7.51 – 7.48 (m, 4H), 7.34 (d, *J* = 8.1 Hz, 1H), 7.18 (d, *J* = 1.9 Hz, 1H), 7.07 (t, *J* = 7.5 Hz, 1H), 6.99 – 6.92 (m, 2H), 3.49 (dd, *J* = 13.4, 6.9 Hz, 2H), 2.89 (t, *J* = 7.4 Hz, 2H), 2.14 (s, 6H, $2CH_3$). ^{13}C NMR (100 MHz, DMSO-d_6): δ 165.60, 161.65, 158.34, 154.08, 144.40, 136.71, 133.19, 133.09, 133.04, 130.33, 127.70, 124.15, 123.08, 121.38, 119.72, 119.04, 119.03, 118.74, 118.68, 112. 31, 111.83, 109.21, 103.59, 99.98, 25.72, 16.24. ESI-MS: *m/z* 554.4 $[M + H]^+$, $C_{33}H_{27}N_7O_2$ (553.22).

(*E*)-3-(4-(4-cyano-2,6-dimethylphenoxy)-2-((4-cyanophenyl)amino)pyrimidin-5-yl)-N-(2-(2-hydroxyethoxy)ethyl)acrylamide (14h)

White powder, yield: 79.6%; mp: 234–236 °C; ^{1}H NMR (400 MHz, DMSO-d_6): δ 10.41 (s, 1H, NH), 8.76 (s, 1H, C_6-pyrimidine-H), 8.25 (t, *J* = 5.5 Hz, 1H, NHCO), 7.84 (s, 2H), 7.53 – 7.49 (m, 1H), 7.49 - 7.48 (m, 4H), 6.97 (d, *J* = 15.9 Hz, 1H, alkene-H), 4.60 (t, *J* = 5.5 Hz, 1H, OH), 3.55 – 3.46 (m, 4H), 3.44 (t, *J* = 5.1 Hz, 2H), 2.14 (s, 6H, $2CH_3$). ^{13}C NMR (100 MHz, DMSO-d_6): δ 165.75, 165.61, 161.70,

158.35, 154.07, 144.38, 133.18, 133.10, 133.03, 130.53, 123.94, 119.71, 118.89, 109.20, 108.33, 103.60, 72.59, 69.59, 60.65, 16.24. ESI-MS: *m/z* 499.4 $[M + H]^+$, $C_{27}H_{26}N_6O_4$ (498.20).

(*E*)-4-((2-((4-cyanophenyl)amino)-5-(3-morpholino-3-oxoprop-1-en-1-yl)pyrimidin-4-yl)oxy)-3,5-dimethylbenzonitrile (14i)

White powder, yield: 77.1%; mp: 283–285 °C; ^{1}H NMR (400 MHz, DMSO-d_6): δ 10.48 (s, 1H, NH), 9.05 (s, 1H, C_6-pyrimidine-H), 7.83 (s, 2H), 7.72 (d, *J* = 15.5 Hz, 1H, alkene-H), 7.47 (d, *J* = 7.2 Hz, 4H), 7.38 (d, *J* = 15.5 Hz, 1H, alkene-H), 3.70 – 3.45 (m, 8H), 2.13 (s, 6H, $2CH_3$). ^{13}C NMR (101 MHz, DMSO-d_6): δ 165.46, 164.98, 160.37, 158.78, 154.05, 144.33, 133.18, 133.14, 133.01, 132.34, 119.68, 119.01, 118.86, 118.00, 109.20, 108.08, 103.65, 66.67, 46.01, 42.66, 16.23. ESI-MS: *m/z* 479.25 $[M - H]^-$ $C_{27}H_{24}N_6O_3$ (480.19).

***Tert*-butyl**

(*E*)-4-(3-(4-(4-cyano-2,6-dimethylphenoxy)-2-((4-cyanophenyl)amino)pyrimidin-5-yl)acrylamido)piperidine-1-carboxylate (15a)

White powder, yield: 80.6%; mp: 266–268 °C; ^{1}H NMR (400 MHz, DMSO-d_6): δ 10.40 (s, 1H, NH), 8.76 (s, 1H, C_6-pyrimidine-H), 8.13 (d, *J* = 7.6 Hz, 1H, NHCO), 7.84 (s, 2H), 7.52 – 7.48 (m, 5H), 6.91 (d, *J* = 15.9 Hz, 1H, alkene-H), 3.88 – 3.85 (m, 3H), 2.92 – 2.88 (m, 2H), 1.79 (d, *J* = 12.1 Hz, 2H, piperazine-2H), 1.40 (s, 9H, Boc-9H), 1.26 (dd, *J* = 24.7, 12.8 Hz, 2H, piperazine-2H). ^{13}C NMR (100 MHz, DMSO-d_6): δ 165.63, 164.84, 161.87, 158.34, 154.40, 154.06, 144.37, 133.19, 133.09, 133.02, 130.70, 124.05, 119.70, 119.01, 118.91, 109.24, 108.33, 103.63, 79.10, 46.30,

31.90, 28.55, 16.25. ESI-MS: m/z 592.32 [M - H]$^-$, $C_{33}H_{35}N_7O_4$ (593.28).

***Tert*-butyl**

(*E*)-4-((3-(4-(4-cyano-2,6-dimethylphenoxy)-2-((4-cyanophenyl)amino)pyrimidin-5-yl)acrylamido)methyl)piperidine-1-carboxylate (15b)

White powder, yield: 79.6%; mp: 271–273 °C; ^{1}H NMR (400 MHz, DMSO-d_6): δ 10.39 (s, 1H, NH), 8.75 (s, 1H, C_6-pyrimidine-H), 8.17 (t, *J* = 5.3 Hz, 1H, NHCO), 7.83 (s, 2H), 7.52 (s, 1H), 7.52– 7.48 (m, 4H), 6.95 (d, *J* = 15.9 Hz, 1H, alkene-H), 3.93 (d, *J* = 11.5 Hz, 2H, piperidine-2H), 3.09 (s, 2H, piperidine-2H), 2.68 (d, *J* = 6.7 Hz, 2H, CH_2), 2.14 (s, 6H, 2CH_3), 1.64 – 1.62 (m, 3H, piperidine-3H), 1.39 (s, 9H, Boc-9H), 1.09 – 0.93 (m, 2H, piperidine-2H). ^{13}C NMR (101 MHz, DMSO-d_6): δ 165.74, 165.60, 161.68, 158.35, 154.35, 154.08, 144.38, 133.18, 133.1, 133.02, 130.47, 123.97, 119.70, 119.01, 118.90, 109.23, 108.35, 103.62, 78.90, 60.21, 44.60, 36.29, 29.96, 28.57, 21.22, 16.24, 14.55. ESI-MS: *m/z* 606.47 [M - H]$^-$, $C_{34}H_{37}N_7O_4$ (607.29).

***Tert*-butyl**

(*E*)-3-(3-(4-(4-cyano-2,6-dimethylphenoxy)-2-((4-cyanophenyl)amino)pyrimidin-5-yl)acrylamido)pyrrolidine-1-carboxylate (15c)

White powder, yield: 80.1%; mp: 253–255 °C; ^{1}H NMR (400 MHz, DMSO-d_6): δ 10.41 (s, 1H, NH), 8.76 (s, 1H, C_6-pyrimidine-H), 8.40 (d, *J* = 5.7 Hz, 1H, NHCO), 7.84 (s, 2H), 7.54 (s, 1H), 7.50 – 7.48 (m, 4H), 6.93 (d, *J* = 15.8 Hz, 1H, alkene-H), 4.33 (d, *J* = 4.8 Hz, 1H), 3.50 (dd, *J* = 17.5, 11.4 Hz, 1H), 3.11 (d, *J* = 10.7 Hz, 1H), 2.90 (s, 1H), 2.74 (s, 1H), 2.14 (s, 6H, 2CH_3), 2.10 – 2.01 (m, 1H, pyrrolidine-H),

1.79 (d, *J* = 5.4 Hz, 1H, pyrrolidine-H), 1.40 (s, 9H, Boc-9H). ^{13}C NMR (100 MHz, DMSO-d_6): δ 165.66, 165.60, 161.99, 158.38, 154.06, 153.97, 144.35, 133.19, 133.09, 133.02, 130.99, 123.59, 119.69, 119.00, 118.93, 109.25, 108.26, 103.66, 78.81, 55.36, 48.78, 44.45, 28.64, 16.24. ESI-MS: *m/z* 578.36 [M - H]$^-$, $C_{32}H_{33}N_7O_4$ (579.26).

***Tert*-butyl**

(*E*)-3-((3-(4-(4-cyano-2,6-dimethylphenoxy)-2-((4-cyanophenyl)amino)pyrimidin-5-yl)acrylamido)methyl)pyrrolidine-1-carboxylate (15d)

White powder, yield: 82.6%; mp: 256–258 °C; ^{1}H NMR (400 MHz, DMSO-d_6): δ 10.41 (s, 1H, NH), 8.77 (s, 1H, C_6-pyrimidine-H), 8.27 (s, 1H, NHCO), 7.84 (s, 2H), 7.54 (s, 1H), 7.50 – 7.49 (m, 4H), 6.94 (d, *J* = 15.8 Hz, 1H, alkene-H), 3.46 – 3.44 (d, *J* = 6.8 Hz, 1H), 3.28 – 3.11 (m, 3H), 3.03 – 2.91 (m, 1H), 2.74 – 2.70 (m, 1H), 2.40 – 2.26 (m, 1H), 2.14 (s, 6H, 2CH_3), 1.91 (s, 1H, pyrrolidine-H), 1.57 (dd, *J* = 23.3, 11.0 Hz, 1H, pyrrolidine-H), 1.39 (s, 9H, Boc-9H). ^{13}C NMR (100 MHz, DMSO-d_6): δ 165.81, 165.61, 161.76, 158.36, 154.07, 154.00, 144.37, 133.20, 133.09, 133.02, 130.66, 123.77, 119.70, 119.02, 118.90, 109.23, 108.30, 103.61, 78.61, 49.73, 49.52, 45.49, 45.35, 41.38, 29.36, 28.67, 16.24. ESI-MS: *m/z* 592.44 [M - H]$^-$, $C_{33}H_{35}N_7O_4$ (593.28).

***Tert*-butyl**

(*E*)-4-(3-(4-(4-cyano-2,6-dimethylphenoxy)-2-((4-cyanophenyl)amino)pyrimidin-5-yl)acryloyl)piperazine-1-carboxylate (15e)

White powder, yield: 83.4%; mp: 261–263 °C; ^{1}H NMR (400 MHz, DMSO-d_6): δ 10.30 (s, 1H, NH), 8.55 (s, 1H, C_6-pyrimidine-H), 7.80 (s, 2H), 7.48 (s, 4H), 6.86 (d, *J*

= 12.5 Hz, 1H, alkene-H), 6.42 (d, *J* = 12.5 Hz, 1H, alkene-H),3.46 – 3.45 (m, 4H, piperazine-4H), 3.30 – 3.18 (m, 4H, piperazine-4H), 2.11 (s, 6H, $2CH_3$), 1.37 (s, 9H, Boc-9H). ^{13}C NMR (100 MHz, DMSO-d_6): δ 166.44, 164.79, 159.80, 158.42, 154.24, 153.98, 144.51, 133.16, 133.02, 125.54, 125.02, 119.73, 118.98, 118.77, 109.16, 108.49, 103.44, 79.70, 45.87, 40.97, 28.45, 16.19. ESI-MS: *m/z* 578.28 $[M + H]^+$, $C_{32}H_{33}N_7O_4$ (579.26).

***Tert*-butyl**

(*E*)-4-(2-(3-(4-(4-cyano-2,6-dimethylphenoxy)-2-((4-cyanophenyl)amino)pyrimidin-5-yl)acrylamido)ethyl)piperazine-1-carboxylate (15f)

White powder, yield: 79.8%; mp: 286–288°C; ^{1}H NMR (400 MHz, DMSO-d_6): δ 10.41 (s, 1H, NH), 8.77 (s, 1H, C_6-pyrimidine-H), 8.13 (t, *J* = 4.6 Hz, 1H, NHCO), 7.84 (s, 2H), 7.52–7.48 (m, 5H), 6.94 (d, *J* = 15.7 Hz, 1H, alkene-H), 3.32 – 3.31 (m, 6H), 2.42 (t, *J* = 6.1 Hz, 2H), 2.35 (s, 4H, piperazine-4H), 2.14 (s, 6H, $2CH_3$), 1.40 (s, 9H, Boc-9H). ^{13}C NMR (101 MHz, DMSO-d_6): δ 165.62, 165.59, 161.63, 158.36, 154.26, 154.07, 144.38, 133.19, 133.09, 133.02, 130.43, 123.92, 119.71, 119.02, 118.88, 109.22, 108.30, 103.60, 79.19, 57.53, 52.97, 36.70, 28.53, 16.24. ESI-MS: *m/z* 623.11 $[M + H]^+$ $C_{34}H_{38}N_8O_4$ (622.30).

(*E*)-4-((5-(3-(4-acetylpiperazin-1-yl)-3-oxoprop-1-en-1-yl)-2-((4-cyanophenyl)amino)pyrimidin-4-yl)oxy)-3,5-dimethylbenzonitrile (17j)

White powder, yield: 79.2%; mp: 277–279 °C; ^{1}H NMR (400 MHz, DMSO-d_6): δ 10.48 (s, 1H, NH), 9.05 (s, 1H, C_6-pyrimidine-H), 7.82 (s, 2H), 7.71 (d, *J* = 15.5 Hz, 1H, alkene-H),7.49 – 7.46 (m, 4H), 7.40 (d, *J* = 15.6 Hz, 1H, alkene-H), 3.80 – 3.60

(m, 4H, piperazine-4H), 3.56 – 3.49 (m, 4H, piperazine-4H), 2.12 (s, 6H, $2CH_3$), 2.04 (s, 3H, CH_3). ^{13}C NMR (100 MHz, DMSO-d_6): δ 168.95, 165.47, 165.05, 158.79, 154.05, 144.33, 133.19, 133.15, 133.01, 119.69, 119.01, 118.88, 109.20, 108.07, 103.66, 55.37, 21.74, 16.24. ESI-MS: *m/z* 520.33 $[M - H]^-$, $C_{29}H_{27}N_7O_3$ (521.22).

(E)-4-((2-((4-cyanophenyl)amino)-5-(3-(4-formylpiperazin-1-yl)-3-oxoprop-1-en-1-yl)pyrimidin-4-yl)oxy)-3,5-dimethylbenzonitrile (17k)

White powder, yield: 78.3%; mp: 256–258 °C; ^1H NMR (400 MHz, DMSO-d_6): δ 10.49 (s, 1H, NH), 9.07 (s, 1H, C_6-pyrimidine-H), 8.10 (s, 1H, aldehyde-H), 7.83 (s, 2H), 7.74 (d, *J* = 15.5 Hz, 1H, alkene-H), 7.58 – 7.36 (m, 5H), 3.66 (dd, *J* = 42.6, 22.9 Hz, 4H, piperazine-4H), 3.45 (s, 4H, piperazine-4H), 2.13 (s, 6H, $2CH_3$). ^{13}C NMR (100 MHz, DMSO-d_6): δ 165.45, 165.06, 161.60, 160.25, 158.83, 154.05, 144.32, 133.19, 133.15, 133.02, 132.46, 119.69, 119.02, 118.87, 117.98, 109.19, 108.01, 103.66, 55.38, 45.13, 16.24. ESI-MS: *m/z* 506.38 $[M - H]^-$, $C_{28}H_{25}N_7O_3$ (507.20).

*General procedure for the synthesis of target compounds **17a–i** and **17l.***

To a solution of **15a–f** (0.16 mmol) in DCM (10 mL) was added trifluoroacetic acid (TFA) (0.8 mmol) at room temperature, and the solution was stirred for 4 h (monitored by TLC). After adjusting the pH of the mixture to 9-10 with saturated sodium bicarbonate solution and washed with water (10 mL), the aqueous phase was extracted with DCM (3 × 10 mL). The combined organic phase was dried over anhydrous Na_2SO_4, filtered, and concentrated under reduced pressure to give the crude product **16a–f**, which was used directly in the next reaction without any further purification. Then the crude product was dissolved in DCM (10mL). The TEA (1.9

mmol) was added to the solution at 0 °C. Sulfonamide or amide dissolved in DCM (1 mL) was added to the mixture after an additional 10 min. The mixture was warmed to room temperature overnight until complete consumption of starting material as monitored by TLC. The solvent was removed under reduced pressure to afford corresponding crude product, which was purified by silica gel chromatography to yield **17a–i** and **17l**.

(*E*)-3-(4-(4-cyano-2,6-dimethylphenoxy)-2-((4-cyanophenyl)amino)pyrimidin-5-yl)-N-(1-(methylsulfonyl)piperidin-4-yl)acrylamide (17a)

White powder, yield: 82.6%; mp: 260–262°C; ^{1}H NMR (400 MHz, DMSO-d_6): δ 10.41 (s, 1H, NH), 8.76 (s, 1H, C_6-pyrimidine-H), 8.22 (d, *J* = 7.5 Hz, 1H, NHCO), 7.84 (s, 2H), 7.54 (s, 1H), 7.50 – 7.48 (m, 4H), 6.92 (d, *J* = 15.9 Hz, 1H, alkene-H), 3.82 – 3.81 (m, 1H), 3.52 (d, *J* = 12.0 Hz, 2H), 2.97 – 2.78 (m, 5H), 2.14 (s, 6H, $2CH_3$), 1.92 (d, *J* = 12.9 Hz, 1H, piperidine-2H), 1.46 (td, *J* = 14.7, 3.8 Hz, 2H, piperidine-2H). ^{13}C NMR (100 MHz, DMSO-d_6): δ 165.65, 165.03, 161.96, 158.36, 154.07, 144.37, 133.21, 133.09, 133.05, 130.87, 123.85, 119.73, 119.05, 118.91, 118.70, 109.23, 108.28, 103.62, 103.34, 45.76, 44.94, 44.86, 34.68, 31.40, 31.23, 16.25. ESI-MS: *m/z* 570.22 $[M - H]^-$, $C_{29}H_{29}N_7O_4S$ (571.20).

(*E*)-3-(4-(4-cyano-2,6-dimethylphenoxy)-2-((4-cyanophenyl)amino)pyrimidin-5-yl)-N-((1-(methylsulfonyl)piperidin-4-yl)methyl)acrylamide (17b)

White powder, yield: 80.9%; mp: 175–177 °C; ^{1}H NMR (400 MHz, DMSO-d_6): δ 10.40 (s, 1H, NH), 8.76 (s, 1H, C_6-pyrimidine-H), 8.22 (t, *J* = 5.5 Hz, 1H, NHCO), 7.84 (s, 2H), 7.53 – 7.49 (m, 5H), 6.96 (d, *J* = 15.9 Hz, 1H, alkene-H), 3.56 (d, *J* =

11.0 Hz, 2H, piperidine-2H), 3.13 (t, *J* = 5.8 Hz, 2H, piperidine-2H), 2.84 (s, 3H, CH_3), 2.67 (t, *J* = 11.6 Hz, 2H, CH_2), 2.14 (s, 6H, $2CH_3$), 1.76 (d, *J* = 12.9 Hz, 2H, piperidine-2H), 1.58 (s, 1H, piperidine-H), 1.20 (dd, *J* = 21.5, 10.6 Hz, 2H, piperidine-2H). ^{13}C NMR (100 MHz, DMSO-d_6): δ 165.78, 165.59, 161.64, 158.35, 154.09, 144.39, 133.19, 133.11, 133.02, 130.45, 123.93, 119.72, 119.03, 118.89, 118.69, 109.21, 108.32, 103.58, 99.98, 45.76, 44.32, 35.55, 34.50, 29.51, 16.26. ESI-MS: *m/z* 587.32 $[M + H]^+$, $C_{30}H_{31}N_7O_4S$ (585.22)

(*E*)-3-(4-(4-cyano-2,6-dimethylphenoxy)-2-((4-cyanophenyl)amino)pyrimidin-5-yl)-N-(1-((trifluoromethyl)sulfonyl)piperidin-4-yl)acrylamide (17c)

White powder, yield: 70.6%; mp: 294–296 °C; ^{1}H NMR (400 MHz, DMSO-d_6): δ 10.42 (s, 1H, NH), 8.77 (s, 1H, C_6-pyrimidine-H), 8.25 (d, *J* = 7.6 Hz, 1H, NHCO), 7.84 (s, 2H), 7.54 (s, 1H), 7.50 – 7.48 (m, 4H), 6.90 (d, *J* = 15.9 Hz, 1H, alkene-H), 4.08 – 3.91 (m, 1H), 3.77 (d, *J* = 13.1 Hz, 2H), 3.40 (m, 2H), 2.13 – 1.94 (m, 2H, piperazine-4H), 1.45 (td, *J* = 14.5, 4.1 Hz, 2H, piperazine-2H). ^{13}C NMR (100 MHz, DMSO-d_6): δ 165.76, 165.65, 165.12, 163.51(d, $^1J_{CF}$ = 303 Hz), 158.37, 154.04, 144.36, 133.21, 133.08, 133.03, 131.01, 123.73, 119.70, 119.01, 118.92, 118.53, 109.25, 108.25, 103.64, 45.77, 44.91, 31.64, 16.25. ESI-MS: *m/z* 626.4 $[M + H]^+$, 643.4 $[M + NH_4]^+$, $C_{29}H_{26}F_3N_7O_4S$ (625.17)

(E)-3-(4-(4-cyano-2,6-dimethylphenoxy)-2-((4-cyanophenyl)amino)pyrimidin-5-yl)-N-(1-(2,2,2-trifluoroacetyl)piperidin-4-yl)acrylamide (17d)

White powder, yield: 76.2%; mp: 141–143 °C; ^{1}H NMR (400 MHz, DMSO-d_6): δ 10.41 (s, 1H, NH), 8.76 (s, 1H, C_6-pyrimidine-H), 8.21 (d, *J* = 7.5 Hz, 1H, NHCO),

7.84 (s, 2H), 7.54 (s, 1H), 7.51 – 7.48 (m, 4H), 6.91 (d, *J* = 15.9 Hz, 1H, alkene-H), 4.19 – 4.16 (m, 1H), 4.12 – 3.97 (m, 1H), 3.85 – 3.81 (m, 1H), 3.41 (t, *J* = 11.9 Hz, 1H), 3.14 (t, *J* = 11.4 Hz, 1H), 2.05 – 1.85 (m, 2H), 1.44 – 1.34 (m, 2H). ^{13}C NMR (100 MHz, DMSO-d_6): δ 167.87, 167.22, 164.19, 160.58, 156.71(d, $^{2}J_{CF}$= 35.3 Hz), 156.26, 146.79, 146.58, 135.42, 135.39, 135.30, 135.25, 133.17, 126.02, 121.93, 121.24, 121.13, 120.92, 119.11(d, $^{1}J_{CF}$ = 289.9 Hz), 111.46, 110.49, 105.85, 47.88, 46.69, 44.67, 34.49, 33.56, 18.45, 18.43. ESI-MS: *m/z* 590.4 $[M + H]^+$, 607.4 $[M + NH_4]^+$, $C_{30}H_{26}F_3N_7O_3$ (589.20).

(*E*)-3-(4-(4-cyano-2,6-dimethylphenoxy)-2-((4-cyanophenyl)amino)pyrimidin-5-yl)-N-(1-(methylsulfonyl)pyrrolidin-3-yl)acrylamide (17e)

White powder, yield: 77.3%; mp: 158–160 °C; ^{1}H NMR (400 MHz, DMSO-d_6): δ 10.43 (s, 1H, NH), 8.77 (s, 1H, C_6-pyrimidine-H), 8.46 (d, *J* = 6.5 Hz, 1H, NHCO), 7.85 (s, 2H), 7.55 (s, 1H), 7.51 – 7.48 (m, 4H), 6.94 (d, *J* = 15.8 Hz, 1H, alkene-H), 4.39 (dd, *J* = 11.2, 5.7 Hz, 1H), 3.51 (dd, *J* = 10.2, 6.4 Hz, 1H), 3.41 – 3.32 (m, 4H), 3.09 (dd, *J* = 10.2, 4.3 Hz, 1H), 2.91 (s, 3H, CH_3), 2.23 – 2.07 (m, 7H, $2CH_3$, pyrrolidine-H), 1.85 (td, *J* = 12.6, 6.1 Hz, 1H, pyrrolidine-H). ^{13}C NMR (101 MHz, DMSO-d_6): δ 165.68, 162.11, 158.39, 154.05, 144.34, 133.21, 133.08, 133.03, 131.22, 123.40, 119.70, 119.01, 118.93, 109.25, 108.22, 103.66, 53.21, 49.59, 46.47, 33.86, 31.36, 16.24. ESI-MS: *m/z* 556.39 $[M - H]^-$, $C_{28}H_{27}N_7O_4S$ (557.18).

(*E*)-3-(4-(4-cyano-2,6-dimethylphenoxy)-2-((4-cyanophenyl)amino)pyrimidin-5-yl)-N-((1-(methylsulfonyl)pyrrolidin-3-yl)methyl)acrylamide (17f)

White powder, yield: 76.8%; mp: 264–266 °C; ^{1}H NMR (400 MHz, DMSO-d_6): δ 10.42 (s, 1H, NH), 8.77 (s, 1H, C_6-pyrimidine-H), 8.31 (t, *J* = 5.7 Hz, 1H, NHCO), 7.85 (s, 2H), 7.55 (s, 1H), 7.51 – 7.48 (m, 4H), 6.93 (d, *J* = 15.9 Hz, 1H, alkene-H), 3.33 – 3.16 (m, 5H), 2.99 – 2.95 (m, 1H), 2.90 (s, 3H, CH_3), 2.39 (dt, *J* = 14.3, 7.3 Hz, 1H, pyrrolidine-H), 2.14 (s, 6H, $2CH_3$), 1.98 (dt, *J* = 12.5, 6.7 Hz, 1H, pyrrolidine-H), 1.64 (dt, *J* = 18.0, 6.6 Hz, 1H, pyrrolidine-H). ^{13}C NMR (100 MHz, DMSO-d_6): δ 165.86, 165.63, 161.83, 158.37, 154.06, 144.37, 133.20, 133.09, 133.03, 130.82, 123.66, 119.71, 119.02, 118.91, 109.24, 108.27, 103.63, 55.37, 51.36, 47.39, 41.33, 33.60, 29.38, 16.25. ESI-MS: *m/z* 571.89 $[M + H]^+$, $C_{29}H_{29}N_7O_4S$ (571.20).

(*E*)-4-((2-((4-cyanophenyl)amino)-5-(3-(4-(methylsulfonyl)piperazin-1-yl)-3-oxoprop-1-en-1-yl)pyrimidin-4-yl)oxy)-3,5-dimethylbenzonitrile (17g)

White powder, yield: 75.4%; mp: 200–202 °C; ^{1}H NMR (400 MHz, DMSO-d_6): δ 10.49 (s, 1H, NH), 9.07 (s, 1H, C_6-pyrimidine-H), 7.83 (s, 2H), 7.74 (d, *J* = 15.5 Hz, 1H, alkene-H), 7.48 – 7.47 (m, 4H), 7.42 (d, *J* = 15.5 Hz, 1H, alkene-H), 3.77 (d, *J* = 45.2 Hz, 1H, piperazine-4H), 3.17 (s, 4H, piperazine-4H), 2.91 (s, 3H, CH_3), 2.13 (s, 6H, $2CH_3$). ^{13}C NMR (100 MHz, DMSO-d_6): δ 166.32, 165.49, 165.00, 164.76, 160.41, 158.84, 158.42, 154.06, 144.32, 133.22, 133.17, 133.04, 132.71, 118.88, 118.77, 117.83, 109.20, 103.67, 45.70, 34.55, 16.25. ESI-MS: *m/z* 556.13 $[M - H]^-$, $C_{28}H_{27}N_7O_4S$ (557.18).

(*E*)-4-((2-((4-cyanophenyl)amino)-5-(3-oxo-3-(4-((trifluoromethyl)sulfonyl)piperazin-1-yl)prop-1-en-1-yl)pyrimidin-4-yl)oxy)-3,5-dimethylbenzonitrile (17h)

White powder, yield: 79.6%; mp: 292–294 °C; ^{1}H NMR (400 MHz, DMSO-d_6): δ 10.49 (s, 1H, NH), 9.03 (s, 1H, C_6-pyrimidine-H), 7.83 (s, 2H), 7.72 (d, J = 15.5 Hz, 1H, alkene-H), 7.48 – 7.40 (m, 4H), 7.38 (d, J = 15.5 Hz, 1H, alkene-H), 3.85 – 3.82 (m, 4H, piperazine-4H), 3.55 (s, 4H, piperazine-4H), 2.12 (s, 6H, $2CH_3$). ^{13}C NMR (100 MHz, DMSO-d_6): δ 166.53, 165.51, 164.68, 161.12(d, $^{1}J_{CF}$ = 185.84 Hz), 158.44, 153.91, 144.49, 144.29, 133.17, 133.03, 126.54, 124.68, 119.73, 118.97, 118.89, 118.78, 109.20, 108.39, 103.46, 55.37, 46.68, 46.47, 45.90, 16.20. ESI-MS: *m/z* 610.31 $[M - H]^-$, $C_{28}H_{24}F_3N_7O_4S$ (611.16).

(*E*)-4-((2-((4-cyanophenyl)amino)-5-(3-oxo-3-(4-(2,2,2-trifluoroacetyl)piperazin-1-yl)prop-1-en-1-yl)pyrimidin-4-yl)oxy)-3,5-dimethylbenzonitrile (17i)

White powder, yield: 73.5%; mp: 285–287 °C; ^{1}H NMR (400 MHz, DMSO-d_6): δ 10.29 (s, 1H, NH), 8.58 (s, 1H, C_6-pyrimidine-H), 7.80 (s, 2H), 7.48 (s, 4H), 6.90 (d, J = 12.5 Hz, 1H, alkene-H), 6.47 – 6.43 (m, 1H), 3.69 – 3.47 (m, 8H), 2.12 (s, 6H, $2CH_3$). ^{13}C NMR (100 MHz, DMSO-d_6): δ 166.45, 164.86, 159.83, 158.46, 154.83(d, $^{2}J_{CF}$= 32.32 Hz), 153.98, 144.52, 133.16, 133.03, 126.14, 124.52, 119.74, 119.01, 117.00(d, $^{1}J_{CF}$ = 358.5 Hz), 109.14, 108.36, 103.43, 45.78, 45.15, 43.55, 41.04, 16.21, 16.19. ESI-MS: *m/z* 576.3 $[M + H]^+$, $C_{29}H_{24}F_3N_7O_3$ (575.19).

(*E*)-3-(4-(4-cyano-2,6-dimethylphenoxy)-2-((4-cyanophenyl)amino)pyrimidin-5-yl)-N-(2-(4-(methylsulfonyl)piperazin-1-yl)ethyl)acrylamide (17l)

White powder, yield: 76.4%; mp: 277–279 °C; ^{1}H NMR (400 MHz, DMSO-d_6): δ 10.42 (s, 1H, NH), 8.77 (s, 1H, C_6-pyrimidine-H), 8.15 (t, J = 5.4 Hz, 1H, NHCO), 7.85 (s, 2H), 7.53 (s, 1H), 7.49 (s, 4H), 6.93 (d, J = 15.8 Hz, 1H, alkene-H), 3.34–3.29

(m, 4H), 3.10 (s, 4H), 2.87 (s, 3H, CH_3), 2.48–2.45 (m, 4H, piperazine-4H), 2.14 (s, 6H, $2CH_3$). ^{13}C NMR (100 MHz, DMSO-d_6): δ 165.63, 165.60, 161.61, 158.38, 154.06, 144.38, 133.19, 133.09, 133.02, 130.45, 123.89, 119.70, 119.01, 118.91, 109.23, 108.30, 103.63, 57.09, 52.38, 45.84, 36.75, 34.21, 16.24. ESI-MS: *m/z* 601.4 $[M + H]^+$, $C_{30}H_{32}N_8O_4S$ (600.23).

4.2. In Vitro Anti-HIV-1 Assay in TZM-bl Cells and Cytotoxicity Assay [12].

Inhibition of the HIV-1 infection was measured as a reduction in the level of luciferase gene expression after a single round of virus infection of TZM-bl cells as described previously. Briefly, 800 $TCID_{50}$ of the virus (NL4−3) was used to infect TZM-bl cells in the presence of various concentrations of compounds. One day after infection, the culture medium was removed from each well, and 100 μL of Bright Glo reagent (Promega, San Luis Obispo, CA) was added to the cells to measure luminescence using a Victor 2 luminometer. The effective concentration (EC_{50}) against HIV-1 strains was defined as the concentration that caused a 50% decrease in luciferase activity (relative light units) compared to that of control wells.

A CytoTox-Glo cytotoxicity assay (Promega) was used to determine the cytotoxicity of the synthesized compounds. Parallel to the antiviral assays, TZM-bl cells were cultured in the presence of various concentrations of the compounds for 1 day. The percent of viable cells was determined by following the protocol provided by the Manufacturer. The 50% cytotoxic concentration (CC_{50}) was defined as the concentration that caused a 50% reduction in cell viability.

4.3. In Vitro Anti-HIV Activities Assays in MT-4 Cells.

The 3-(4,5-dimethylthiazol-2-yl)-2,5-diphenyltetrazolium bromide (MTT) method was used to evaluate the antiviral activity and cytotoxicity of the synthesized compounds as previously described [21, 22]. At the beginning of each experiment, stock solutions (10×final concentration) of test compounds were added in 25 μL volumes to two series of triplicate wells for allowing simultaneous evaluation of their effects on mock- and HIV-infected cells. Serial 5-fold dilutions of the compounds were made in flat-bottomed 96-well microtiter trays directly, including untreated control HIV-1 and mock infected cell samples for each sample using a Biomek 3000 robot (Beckman Instruments, Fullerton, CA). HIV-1 (IIIB) and mutant HIV-1 strains (RES056, F227L/V106A, L100I, K103N, E138K, Y181C, and Y188L) stock (50 μL at 100−300 $CCID_{50}$) (50% cell culture infectious dose) or culture medium was added to either the infected or mock-infected wells of the microtiter tray. Mock-infected cells were used to evaluate the effect on uninfected cells to assess the cytotoxicity of the test compounds. Exponentially growing MT-4 cells were centrifuged for 5 min at 1000 rpm (Eppendorf 5424, Hamburg, Germany) and then supernatant was discarded. The MT-4 cells were resuspended at 6×10^5 cells/mL, and 50 μL aliquots were transferred to the microtiter tray wells. At 5 days after infection, the viability of mock- and HIV-infected cells was determined spectrophotometrically by means of the MTT assay.

The MTT assay is based on the reduction of yellow-colored MTT (Acros Organics, Geel, Belgium) by mitochondrial dehydrogenase of metabolically active cells to form a blue-purple formazan. The absorbances were read in an eight-channel

computer-controlled photometer at the wavelengths of 540 and 690 nm. All data were calculated using the median optical density (OD) value of three wells. The 50% effective antiviral concentration (EC_{50}) was defined as the concentration of the test compound affording 50% protection from viral cytopathogenicity. The CC_{50} was defined as the compound concentration that reduced the absorbance (OD_{540}) of mock-infected cells by 50%.

4.4. HIV-1 RT Inhibition Assays.

The HIV-1 RT inhibition assay was performed by using an RT assay kit produced by Roche. The procedure for assaying HIV-1 RT inhibition was conducted as the kit protocol [23].

First, the HIV-1 RT enzyme, reconstituted template, and viral nucleotides [digoxigenin (DIG)- dUTP, biotin-dUTP, and dTTP] were incubated for 1 h at 37 °C in the incubation buffer with or without inhibitors. Then the reaction mixture was transferred to a streptavidin-coated microtiter plate (MTP) and incubated for another 1 h at 37 °C. The biotin-labeled dNTPs were incorporated into the cDNA chain in the presence of RT and bound to streptavidin. The washing buffer was used to wash the unbound dNTPs, and add the anti-DIG-POD was added to the MTPs.

After incubation for 1 h at 37 °C, the DIG-labeled dNTPs incorporated in cDNA were bound to the anti-DIG-POD antibody. The peroxide substrate (ABTS) solution was added to the MTPs, when the unbound anti-DIG-PODs were washed out. The reaction mixture was incubated at 25 °C until the green color was sufficiently developed for detection. The absorbance of the sample was determined at OD_{405} nm

using a microtiter plate ELISA reader. The percentage inhibitory activity of RT inhibitors was calculated according to the following formula: % inhibition = [O.D. value with RT but without inhibitors − O.D. value with RT and inhibitors]/[O.D. value with RT and inhibitors−- O.D. value without RT and inhibitors]. The IC_{50} values correspond to the concentrations of the inhibitors required to inhibit biotin-dUTP incorporation by 50%.

4.5. Molecular docking and dynamics simulation

The crystal structure of HIV-1 reverse transcriptase (HIV-1 RT) with an entry of 4KFB was retrieved from the RCSB Protein Data Bank [24]. This 3D structure consisted of a co-crystallized ligand bound at its NNRTI-binding pocket (NNIBP) which was removed, in addition to the one at the NNRTI adjacent site, since they were not of interest in this study. However, the co-crystal ligands were initially used to map out residues located within 5Å radius of the target pockets for docking.

Prior to molecular docking, conformations of our compounds of interest (**14c** and **17l**) were stabilized via full energy optimization and minimization at the B3LYP/6-311++G(d,p) level [25] using the GaussView [26] / Gaussian16 [27] program packages.

Appropriate coordinates (*x, y, z*) for the grid-box were defined for each pockets and the compounds were rationally docked into them. To simulate the differential binding of the compounds at the NNIBP, we obtained two docked complexes as highlighted in **Table 9**. These systems connote ligand-bound HIV-1 RT complexes with the compounds docked differently in the NNIBP.

Table 9: Details of pre-MD system preparation

Systems prepared	Details
14c → NNIPB	**14c** docked into **NNIBP**
17l → NNIBP	**17l** docked into the **NNIBP**

The docked complexes were selected as starting structures for analyses and subjected to molecular dynamics (MD) simulations. We performed a 100ns simulation run on Amber18 Graphical Processor Unit [28] whereby the production runs were accelerated. While protein parameterization was done on FF14SB forcefield, integrated modules such as the LEAP, Antechamber, Parmchk, and pdb4amber were used for ligand parameterization and other functionalities relative to system neutralization, solvation and renaming [29]. Topology and parameter files for the protein, ligand and complexes were generated after which the systems were minimized, initially for 2500 steps with a 500kcal/mol $Å^2$ restraint potential and secondly for 5000 steps with no restraints. Simultaneous heating (0-300k) and equilibration steps were then initiated after which the systems were subjected to 100ns production runs. Resulting trajectories were saved at every 1ns and analyzed using the CPPTRAJ module. We then obtained data plots and snapshots for time-based visual analysis using the Origin analytical software and GUI of UCSF Chimera [30], Biovia Discovery Studio [31] and GIMP 2.0 (for image creation).

The Molecular Mechanics/Generalized Born Surface Area (MM/GBSA) method [32] was used to investigate the binding dynamics of **14c** and **17l** at the HIV-1 RT NNIBP. Also, per-residue energies were decomposed in order to identify important

residues that contribute to the high-affinity binding and stabilization of the compounds at the pocket. These analytical methods were employed to understand the inhibitory potencies of the compounds in their singly- and dually-bound states. More importantly, this approach would enable us to rationally explain if the binding of one compound supersedes the potency of the other, and which compound has likely higher affinity for the NNIBP.

Notes

The authors declare no competing financial interest.

Acknowledgments

We gratefully acknowledge financial support from the National Natural Science Foundation of China (NSFC Nos. 81973181, 81903453), Shandong Provincial Natural Science Foundation (ZR2019BH011), Young Scholars Program of Shandong University (YSPSDU No. 2016WLJH32), Shandong Provincial Key research and development project (Nos. 2017CXGC1401, 2019JZZY021011), the Taishan Scholar Program at Shandong Province and KU Leuven (GOA 10/014)

Conflict of interest

The authors declare no conflict of interest.

References

[1] D. Kang, H. Zhang, Z. Wang, T. Zhao, T. Ginex, F.J. Luque, Y. Yang, G. Wu, D. Feng, F. Wei, J. Zhang, E. De Clercq, C. Pannecouque, C.H. Chen, K.H. Lee, N.A.

Murugan, T.A. Steitz, P. Zhan, X. Liu, Identification of Dihydrofuro[3,4-d]pyrimidine Derivatives as Novel HIV-1 Non-Nucleoside Reverse Transcriptase Inhibitors with Promising Antiviral Activities and Desirable Physicochemical Properties, J. Med. Chem. 62 (2019) 1484-1501.

[2] Y. Tian, Z. Liu, J. Liu, B. Huang, D. Kang, H. Zhang, E. De Clercq, D. Daelemans, C. Pannecouque, K.H. Lee, C.H. Chen, P. Zhan, X. Liu, Targeting the entrance channel of NNIBP: Discovery of diarylnicotinamide 1,4-disubstituted 1,2,3-triazoles as novel HIV-1 NNRTIs with high potency against wild-type and E138K mutant virus, Eur. J. Med. Chem. 151 (2018) 339-350.

[3] D. Kang, D. Feng, T. Ginex, J. Zou, F. Wei, T. Zhao, B. Huang, Y. Sun, S. Desta, E. De Clercq, C. Pannecouque, P. Zhan, X. Liu, Exploring the hydrophobic channel of NNIBP leads to the discovery of novel piperidine-substituted thiophene[3,2-d]pyrimidine derivatives as potent HIV-1 NNRTIs, Acta Pharm. Sin. B, 10 (2020) 878-894.

[4] P. Zhan, C. Pannecouque, E. De Clercq, X. Liu, Anti-HIV Drug Discovery and Development: Current Innovations and Future Trends, J. Med. Chem. 59 (2016) 2849-2878.

[5] H. Zhang, Y. Tian, D. Kang, Z. Huo, Z. Zhou, H. Liu, E. De Clercq, C. Pannecouque, P. Zhan, X. Liu, Discovery of uracil-bearing DAPYs derivatives as novel HIV-1 NNRTIs via crystallographic overlay-based molecular hybridization, Eur. J. Med. Chem. 130 (2017) 209-222.

[6] E.B. Lansdon, K.M. Brendza, M. Hung, R. Wang, S. Mukund, D. Jin, G. Birkus, N.

Kutty, X. Liu, Crystal structures of HIV-1 reverse transcriptase with etravirine (TMC125) and rilpivirine (TMC278): implications for drug design, J. Med. Chem. 53 (2010) 4295-4299.

[7] V. Namasivayam, M. Vanangamudi, V.G. Kramer, S. Kurup, P. Zhan, X. Liu, J. Kongsted, S.N. Byrareddy, The Journey of HIV-1 Non-Nucleoside Reverse Transcriptase Inhibitors (NNRTIs) from Lab to Clinic, J. Med. Chem. 62 (2019) 4851-4883.

[8] E. De Clercq, An Odyssey in antiviral drug development-50 years at the Rega Institute: 1964-2014, Acta Pharm. Sin. B, 5 (2015) 520-543.

[9] Y. Wu, C. Tang, R. Rui, L. Yang, W. Ding, J. Wang, Y. Li, C.C. Lai, Y. Wang, R. Luo, W. Xiao, H. Zhang, Y. Zheng, Y. He, Synthesis and biological evaluation of a series of 2-(((5-akly/aryl-1H-pyrazol-3-yl)methyl)thio)-5-alkyl-6-(cyclohexylmethyl)-pyrimidin-4(3H)-ones as potential HIV-1 inhibitors, Acta Pharm. Sin. B, 10 (2020) 512-528.

[10] K. Jin, M. Liu, C. Zhuang, E. De Clercq, C. Pannecouque, G. Meng, F. Chen, Improving the positional adaptability: structure-based design of biphenyl-substituted diaryltriazines as novel non-nucleoside HIV-1 reverse transcriptase inhibitors, Acta Pharm. Sin. B, 10 (2020) 344-357.

[11] L. Rimsky, J. Vingerhoets, V. Van Eygen, J. Eron, B. Clotet, A. Hoogstoel, K. Boven, G. Picchio, Genotypic and phenotypic characterization of HIV-1 isolates obtained from patients on rilpivirine therapy experiencing virologic failure in the phase 3 ECHO and THRIVE studies: 48-week analysis, J. Acquir. Immune Defic.

Syndr. (1999), 59 (2012) 39-46.

[12] N. Liu, L. Wei, L. Huang, F. Yu, W. Zheng, B. Qin, D.Q. Zhu, S.L. Morris-Natschke, S. Jiang, C.H. Chen, K.H. Lee, L. Xie, Novel HIV-1 Non-nucleoside Reverse Transcriptase Inhibitor Agents: Optimization of Diarylanilines with High Potency against Wild-Type and Rilpivirine-Resistant E138K Mutant Virus, J. Med. Chem. 59 (2016) 3689-3704.

[13] Z. Wang, Z. Yu, D. Kang, J. Zhang, Y. Tian, D. Daelemans, E. De Clercq, C. Pannecouque, P. Zhan, X. Liu, Design, synthesis and biological evaluation of novel acetamide-substituted doravirine and its prodrugs as potent HIV-1 NNRTIs, Bioorg. Med. Chem. 27 (2019) 447-456.

[14] Y. Wang, E. De Clercq, G. Li, Current and emerging non-nucleoside reverse transcriptase inhibitors (NNRTIs) for HIV-1 treatment, Expert Opin. Drug Metab. Toxicol. 15 (2019) 813-829.

[15] D. Kang, Y. Song, W. Chen, P. Zhan, X. Liu, "Old Dogs with New Tricks": exploiting alternative mechanisms of action and new drug design strategies for clinically validated HIV targets, Mol. Biosyst. 10 (2014) 1998-2022.

[16] R.F. Kamil, U. Debnath, S. Verma, Y.S. Prabhakar, Identification of Adjacent NNRTI Binding Pocket in Multi-mutated HIV1- RT Enzyme Model: An in silico Study, Curr. HIV Res. 16 (2018) 121-129.

[17] Z. Huo, H. Zhang, D. Kang, Z. Zhou, G. Wu, S. Desta, X. Zuo, Z. Wang, L. Jing, X. Ding, D. Daelemans, E. De Clercq, C. Pannecouque, P. Zhan, X. Liu, Discovery of Novel Diarylpyrimidine Derivatives as Potent HIV-1 NNRTIs Targeting the "NNRTI

Adjacent" Binding Site, ACS Med Chem Lett, 9 (2018) 334-338.

[18] J. Du, J. Guo, D. Kang, Z. Li, G. Wang, J. Wu, Z. Zhang, H. Fang, X. Hou, Z. Huang, G. Li, X. Lu, X. Liu, L. Ouyang, L. Rao, P. Zhan, X. Zhang, Y. Zhang, New techniques and strategies in drug discovery, Chin. Chem. Lett. 31 (2020) 1695-1708.

[19] D. Kang, Z. Fang, Z. Li, B. Huang, H. Zhang, X. Lu, H. Xu, Z. Zhou, X. Ding, D. Daelemans, E. De Clercq, C. Pannecouque, P. Zhan, X. Liu, Design, Synthesis, and Evaluation of Thiophene[3,2-d]pyrimidine Derivatives as HIV-1 Non-nucleoside Reverse Transcriptase Inhibitors with Significantly Improved Drug Resistance Profiles, J. Med. Chem. 59 (2016) 7991-8007.

[20] S.S. Carroll, D.B. Olsen, C.D. Bennett, L. Gotlib, D.J. Graham, J.H. Condra, A.M. Stern, J.A. Shafer, L.C. Kuo, Inhibition of HIV-1 reverse transcriptase by pyridinone derivatives. Potency, binding characteristics, and effect of template sequence, J. Biol. Chem. 268 (1993) 276-281.

[21] R. Pauwels, J. Balzarini, M. Baba, R. Snoeck, D. Schols, P. Herdewijn, J. Desmyter, E. De Clercq, Rapid and automated tetrazolium-based colorimetric assay for the detection of anti-HIV compounds, J. Virol. Methods, 20 (1988) 309-321.

[22] C. Pannecouque, D. Daelemans, E. De Clercq, Tetrazolium-based colorimetric assay for the detection of HIV replication inhibitors: Revisited 20 years later, Nat. Protoc. 3 (2008) 427-434.

[23] K. Suzuki, B.P. Craddock, N. Okamoto, T. Kano, R.T. Steigbigel, Poly A-linked colorimetric microtiter plate assay for HIV reverse transcriptase, J. Virol. Methods. 44 (1993) 189-198.

[24] J.D. Bauman, D. Patel, C. Dharia, M.W. Fromer, S. Ahmed, Y. Frenkel, R.S. Vijayan, J.T. Eck, W.C. Ho, K. Das, A.J. Shatkin, E. Arnold, Detecting allosteric sites of HIV-1 reverse transcriptase by X-ray crystallographic fragment screening, J. Med. Chem. 56 (2013) 2738-2746.

[25] A.D. Becke, Density-functional thermochemistry. III. The role of exact exchange, The J. Chem. Phys. 98 (1993).

[26] V. GaussView, Dennington, Roy; Keith, Todd A.; Millam, John M. Semichem Inc., Shawnee Mission, KS, 2016. (2016) GaussView 6. Gaussian.

[27] M.J.G. Frisch, Trucks, W., Schlegel, H. B., Scuseria, G. E., Robb, M. A., Cheeseman, J. R., Scalmani, G., Barone, V., Mennucci, B., Petersson, G. A., Nakatsuji, H., Caricato, M., Li, X., Hratchian, H. P., Izmaylov, A. F., Bloino, J., Zheng, G., and Sonnenberg, J. L. (2016) Gaussian 16. Inc. Wallingford, CT.

[28] Case, D. A. (2018) Amber 18. *Univ. California, San Fr.*

[29] D.A. Case, T.E. Cheatham, 3rd, T. Darden, H. Gohlke, R. Luo, K.M. Merz, Jr., A. Onufriev, C. Simmerling, B. Wang, R.J. Woods, The Amber biomolecular simulation programs, J. Comput. Chem. 26 (2005) 1668-1688.

[30] E.F. Pettersen, T.D. Goddard, C.C. Huang, G.S. Couch, D.M. Greenblatt, E.C. Meng, T.E. Ferrin, UCSF Chimera--a visualization system for exploratory research and analysis, J. Comput. Chem. 25 (2004) 1605-1612.

[31] BIOVIA, D. S. (2015) Discovery Studio Modeling Environment. Dassault Systèmes, San Diego.

[32] M. Ylilauri, O.T. Pentikäinen, MMGBSA as a tool to understand the binding

affinities of filamin-peptide interactions, J. Chem. Inf. Model. 53 (2013) 2626-2633.

Table 1. Anti-HIV-1 activity and cytotoxicity of compounds **12** and **14a–i**.

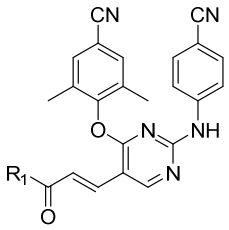

12 and **14a-i**

Compds.	R_1	EC_{50} (nM) [a]	CC_{50} (nM) [b]	SI (NL4-3) [c]
		NL4-3		
12		18.7 ± 3.87	＞227	>12.0
14a		5.36 ± 1.66	＞243	>45.0
14b		5.10 ± 1.22	＞221	>44.0
14c	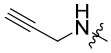	2.45 ± 0.710	＞222	>91.0
14d	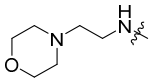	3.44 ± 1.18	＞190	>56.0
14e	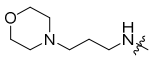	3.53 ± 0.950	＞186	>53.0
14f	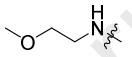	4.48 ± 1.19	＞213	>48.0
14g	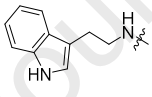	81.3 ± 21.7	**>** 180	>2.00
14h	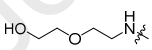	4.81 ± 1.48	**>** 200	>42.0
14i		20.0 ± 5.41	**>** 208	>10.0
7	--	3.77 ± 1.38	**>** 179	>48.0
NVP	--	281 ± 38.7	>15000	>53.0
EFV	--	5.20 ± 0.900	>6300	>1212
ETR	--	1.45 ± 0.500	**>** 229	>158
AZT	--	7.50 ± 1.80	>6300	>1004

[a] EC_{50}: concentration of compound that causes 50% inhibition of viral infection and determined in at least triplicate against HIV-1 virus in TZM-bl cell lines. NL4-3 is wild-type HIV-1 viral strain. [b] CC_{50}: concentration that is cytopathic to 50% of cells. The highest concentration of the tested compounds was 100 ng/mL. [c] SI: selectivity index, the ratio of CC_{50}/EC_{50}.

Table 2. Anti-HIV-1 activity and cytotoxicity of compounds **17a–l**.

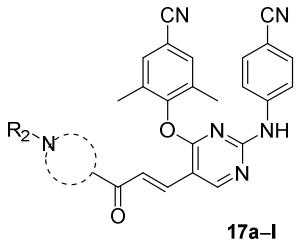

17a–l

Compds.	The group in the dotted circle	R_2	EC_{50} (nM) [a] NL4-3	CC_{50} (nM) [b]	SI (NL4-3) [c]
17a	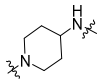		14.2 ± 4.90	**>** 175	>12.0
17b	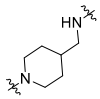		12.8 ± 3.24	**>** 171	>13.0
17c	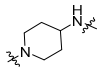		**>** 160	**>** 160	>1.00
17d	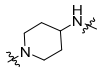		**>** 170	**>** 170	>1.00
17e	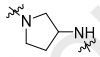		14.7 ± 3.23	**>** 179	>12.0
17f	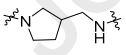		13.6 ± 4.37	**>** 175	>13.0
17g			13.8 ± 5.20	**>** 179	>13.0
17h			**>** 164	**>** 164	>1.00
17i			13.7 ± 2.78	**>** 174	>13.0
17j			49.9 ± 9.78	**>** 192	>4.00
17k			49.3 ± 14.38	**>** 197	>4.00
17l	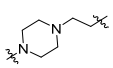		4.16 ± 1.46	**>** 166	>40.0
7	--	--	3.77 ± 1.38	**>** 179	>48.0
NVP	--	--	281 ± 38.7	>15000	>53.0

EFV	--	--	5.20 ± 0.900	>6300	>1212
ETR	--	--	1.45 ± 0.50	**>** 230	>158
AZT	--	--	7.50 ± 1.80	>6300	>1004

[a]EC_{50}: concentration of compound that causes 50% inhibition of viral infection and determined in at least triplicate against HIV-1 virus in TZM-bl cell lines. [b]CC_{50}: concentration that is cytopathic to 50% of cells. The highest concentration of the tested compounds was 100 ng/mL. [c]SI: selectivity index, the ratio of CC_{50}/EC_{50}.

Table 3. Anti-HIV activity and cytotoxicity of **14c–f**, **14h** and **17l**.

Compds.	**EC_{50} (nM)[a]**		**CC_{50} (μM)[b]**	**SI (IIIB)[c]**
	IIIB	**ROD**		
14c	5.20 ± 1.50	> 140538	141 ± 37.7	26934
14d	8.50 ±3.10	> 22383	22.4 ± 7.30	2630
14e	10.5 ± 2.00	> 23027	23.0 ± 10.4	2199
14f	7.80 ± 2.60	> 266797	> 267	> 34341
14h	27.1 ± 10.0	> 61760	61.8 ± 63.4	2278
17l	6.10 ± 1.30	> 5859	5.90 ± 0.800	955
7	3.70 ± 1.40	> 24027	24.0	6535
NVP	84.0 ± 10.7	--	> 9.50	> 113
AZT	18.3 ± 4.2	--	> 7.50	> 410
EFV	2.50 ± 0.800	--	> 6.30	> 2572
ETR	3.00 ± 0.600	--	> 4.60	> 1546

[a]EC_{50}: concentration of compound required to achieve 50% protection of MT-4 cell cultures against HIV-1-induced cytopathic effect, as determined by the MTT method. [b]CC_{50}: concentration required to reduce the viability of mock-infected cell cultures by 50%, as determined by the MTT method. [c]SI: the ratio of CC_{50}/EC_{50}.

Table 4. Anti-HIV activity and cytotoxicity of **14c–f**, **14h** and **17l**.

Compds.	EC_{50} (nM)[a]						
	L100I	**K103N**	**Y181C**	**Y188L**	**E138K**	**F227L/V106A**	**RES056**
14c	113 ± 33.4	10.4 ± 0.600	61.8 ± 13.2	64.5 ± 15.6	10.6 ± 3.00	402 ± 313	1291± 290
14d	263 ± 66.1	18.5 ± 3.60	108 ± 16.2	123 ± 21.0	21.8 ± 4.60	462 ± 87.5	1746 ± 599
14e	254 ± 79.6	22.0 ± 0.700	124 ± 45.7	212 ± 25.6	22.6 ± 5.00	443 ± 415	1209 ± 463
14f	166 ± 50.7	13.7 ± 3.00	98.0 ± 76.5	90.6 ± 17.0	16.5 ± 5.70	343 ± 53.7	1492 ± 563
14h	227 ± 42.7	50.3 ± 14.1	197 ± 34.2	146 ± 3.80	47.1 ± 8.00	318 ± 89.0	1052 ± 372
17l	78.6 ± 31.4	8.70 ± 3.10	48.6 ± 13.1	101 ±24.3	20.9 ± 0.800	251 ± 91.7	808 ± 180
7	16.3 ± 2.80	2.20 ± 0.500	19.1 ± 4.60	38.7 ± 6.10	37.3 ± 9.60	182 ± 121	332 ± 82.0
NVP	373 ± 154	1470 ± 458	2325 ± 1074	3388 ± 1331	72.8 ± 20.6	2730 ± 1258	6748 ± 2323
AZT	7.00 ± 2.60	12.6 ± 3.40	8.70 ± 1.70	9.90 ± 7.80	14.50 ± 2.70	4.70 ± 1.70	20.1 ± 4.70
EFV	30.8 ± 18.4	63.7 ± 14.6	5.20 ± 1.70	148 ± 40.8	5.70 ± 1.20	169 ± 63.9	273 ±153
ETR	10.2 ± 10.3	2.30 ± 0.400	14.0 ± 2.60	15.5 ± 6.80	9.80 ± 3.80	8.20 ± 2.20	60.2 ± 24.7

[a]EC_{50}: concentration of compound required to achieve 50% protection of MT-4 cell cultures against HIV-1-induced cytopathic effect, as determined by the MTT assay.

Table 5. Inhibitory activity against HIV-1 RT (WT).

Compds.	**14c**	**7**	**ETR**
IC_{50} (μM) [a]	0.059	0.035	0.350

[a]IC_{50}: inhibitory concentration of tested compound required to inhibit biotin deoxyuridine triphosphate (biotin-dUTP) incorporation into the HIV-1 (WT) RT by 50%.

Table 6: Estimated values from whole structural analysis and analysis of binding site regions

Systems	Whole Structural Analysis		Binding Site Regions	
	14c → NNIPB	**17l → NNIBP**	**14c → NNIPB**	**17l → NNIBP**
RMSD (Å)	4.6 ± 0.8	4.1 ± 1.2	2.2 ± 0.2	2.1 ± 0.2
RMSF (Å)	2.4 ± 0.8	2.8 ± 1.0	1.6 ± 0.2	1.9 ± 0.4
RoG (Å)	35.4 ± 0.7	35.7 ± 0.7	9.9 ± 0.1	9.6 ± 0.1

Table 7. Estimated values from analysis of ligand motion and dynamics

Systems	14c → NNIPB	17l → NNIBP
RMSD (Å)	1.8 ± 0.4	2.4 ± 0.7
SASA (Å^2)	138.5 ± 0.1	208.1 ± 0.2

Table 8. MM/GBSA energy calculations

Binding energies (kcal/mol)	14c → NNIBP	17l → NNIBP
ΔE_{vdw}	-58.4 ± 0.1	-69.0 ± 0.3
ΔE_{ele}	-2.3 ± 0.2	-43.1 ± 0.4
ΔE_{GB}	25.0 ± 0.2	56.8 ± 0.4
ΔE_{SA}	-7.2 ± 0.01	-8.4 ± 0.01
ΔG_{gas}	-60.8 ± 0.3	-112.2 ± 0.5
ΔG_{sol}	17.8 ± 0.2	48.3 ± 0.4
ΔG_{bind}	-42.9 ± 0.1	-63.9 ± 0.2

ΔE_{ele} = electrostatic energy; **ΔE_{vdW}** = van der Waals energy; **ΔG_{bind}** = total binding free energy; **ΔG_{sol}** = solvation free energy **ΔG_{gas}** = gas phase free energy; **ΔE_{GB}** = polar solvation energy; **ΔE_{SA}** non-polar solvation energy.

Table 9: Details of pre-MD system preparation

Systems prepared	Details
14c → NNIPB	**14c** docked into **NNIBP**
17l → NNIBP	**17l** docked into the **NNIBP**

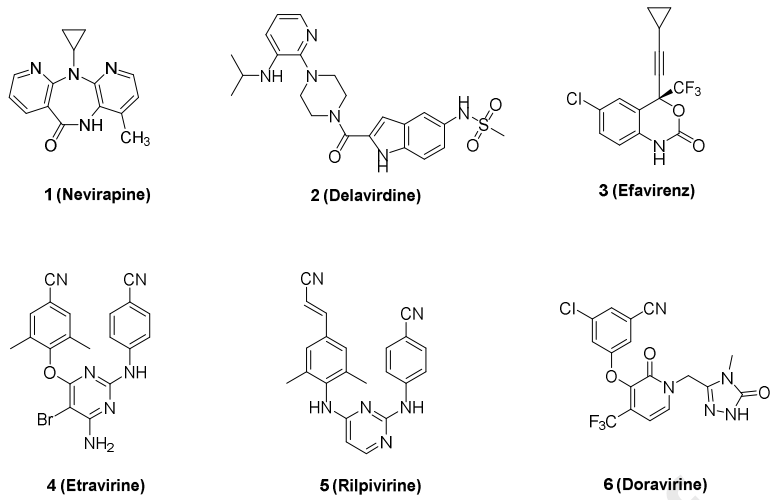

Figure 1. Structures of NNRTIs approved by the US FDA

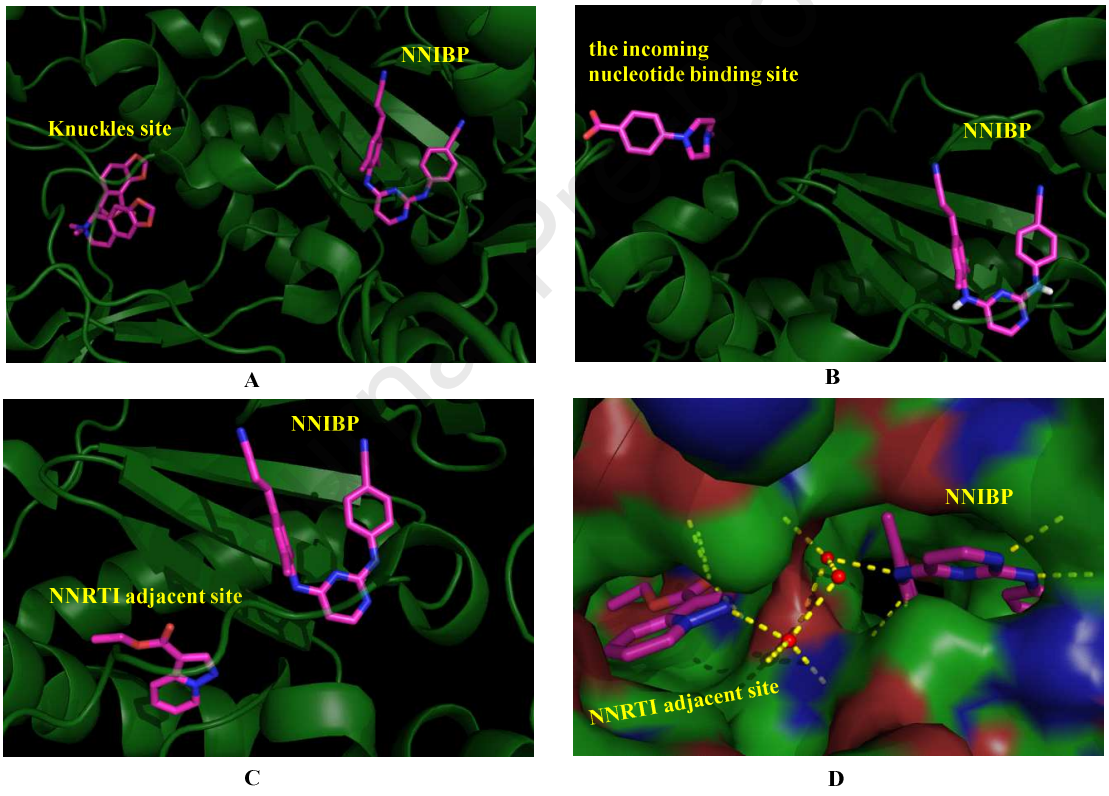

Figure 2. Novel HIV-1 RT binding sites with bound fragments: (A) near Knuckles site (PDB Code: 4IG3); (B) at the incoming nucleotide binding site (PDB Code: 4ICL); (C, D) at NNRTI adjacent site (PDB Code: 4KFB).

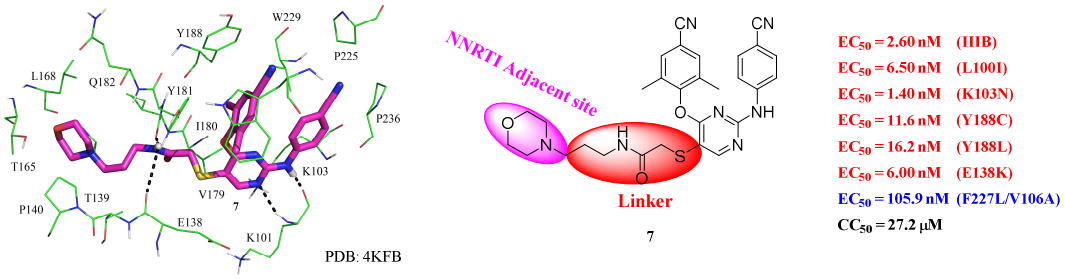

Figure 3. The binding mode and anti-HIV-1 activities of compound **7**.

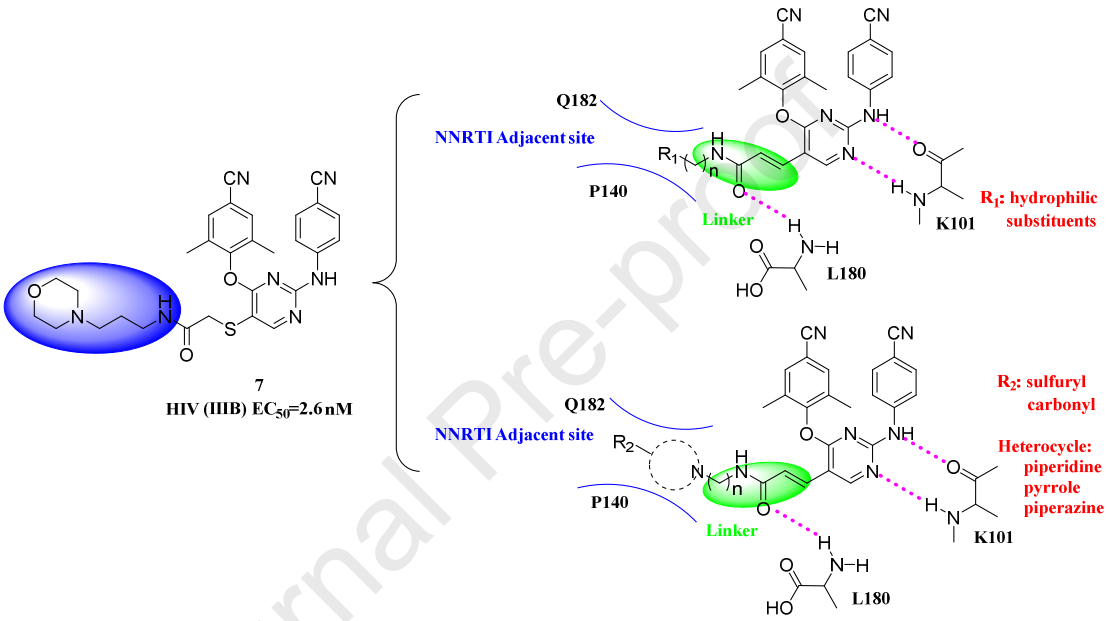

Figure 4. The design of new compounds targeting the NNIBP and the NNRTI adjacent site.

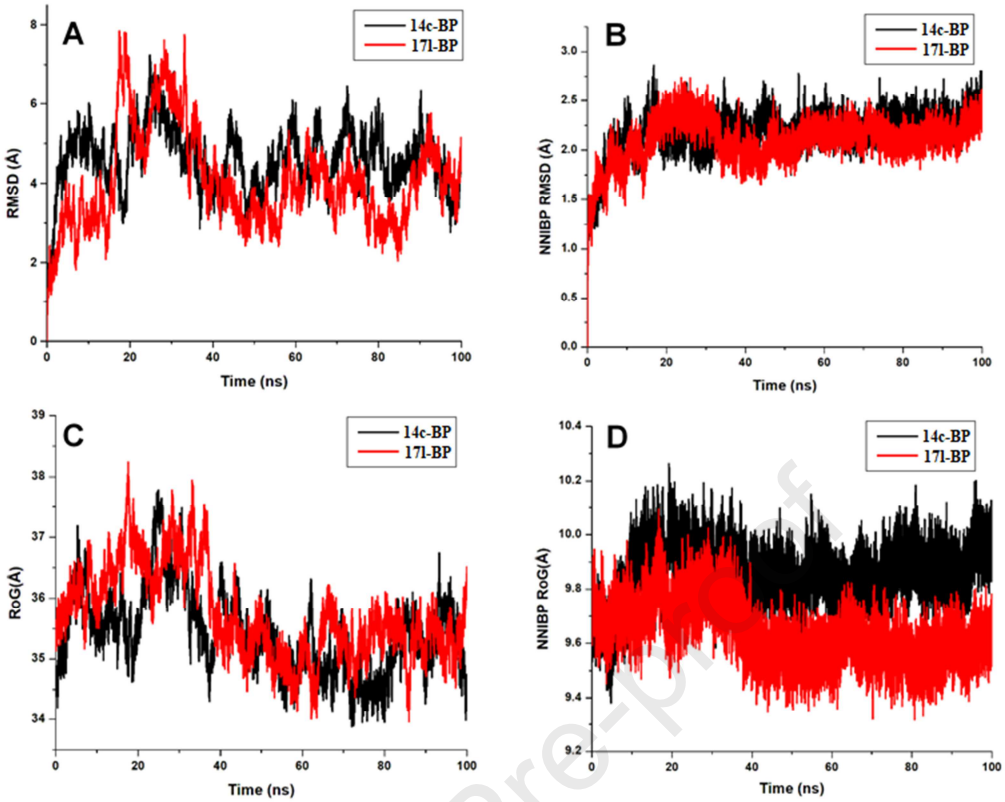

Figure 5. RMSD and RoG analyses for whole protein and NNIBP region in the presence of **14c** (black) and **17l** (red). (A). RMSD analysis of structural stability for entire structure; (B). NNIBP region; (C). RoG analyses for entire protein complex; (D). RoG analysis of NNIBP compactness.

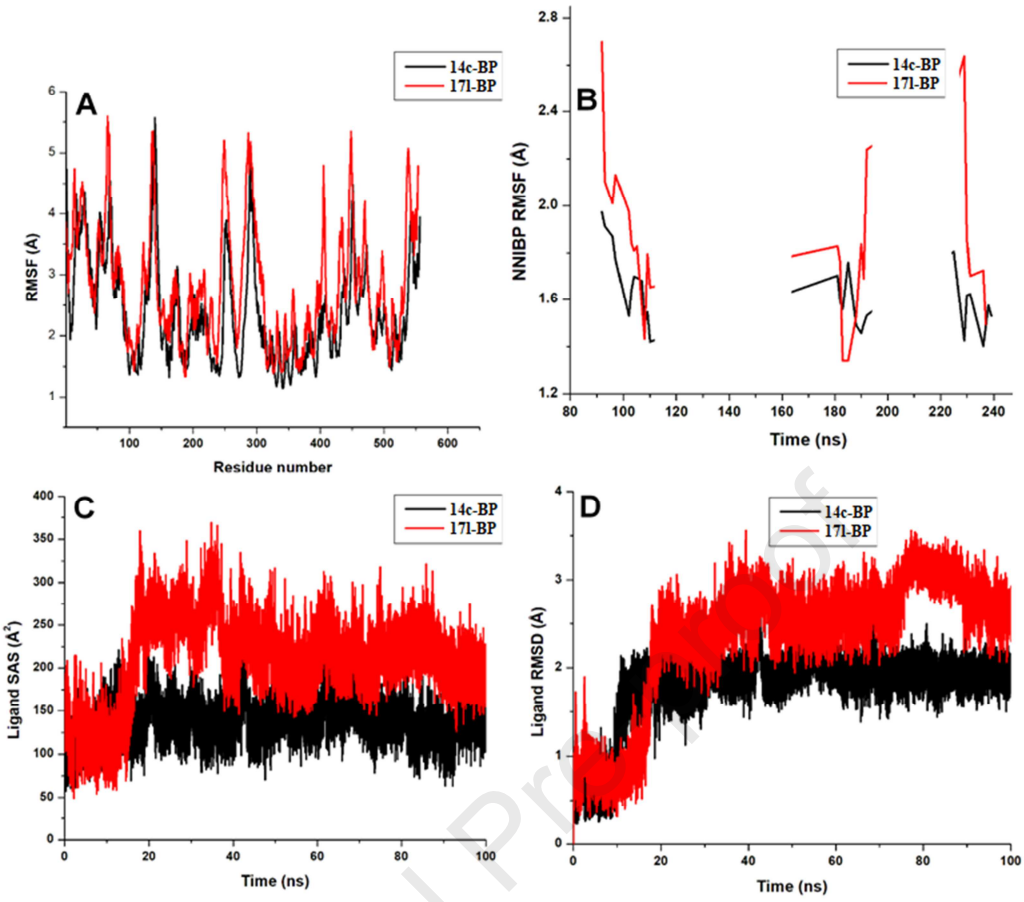

Figure 6. Analyses of per-residual fluctuation in (A). Overall protein structure; (B). NNIBP region. Ligand motions were determined in the **14c** system (black) and **17l** (red) using; (C). SASA analysis; (D). RMSD calculation.

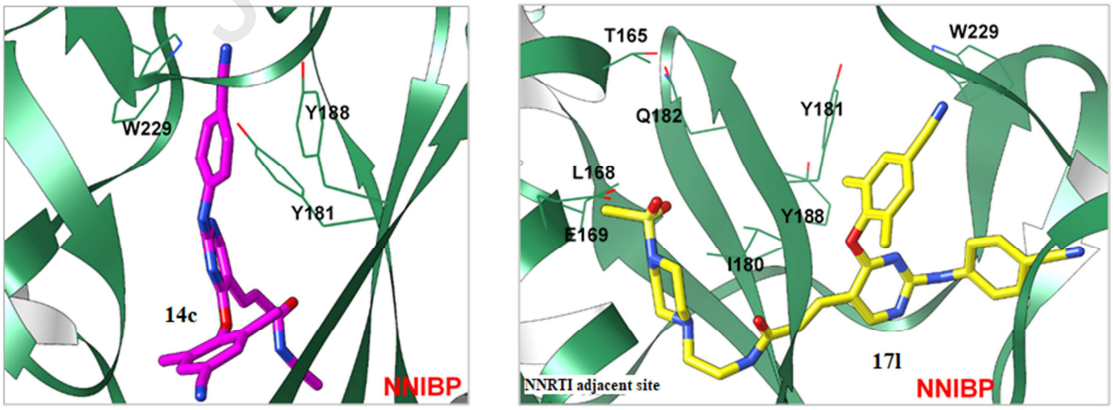

Figure 7. 3D structural representation of **14c** and **17l** positioning at the NNIBP region. The extension of **17l** methyl-sulphonyl piperazine group into the NNRTI adjacent site is shown.

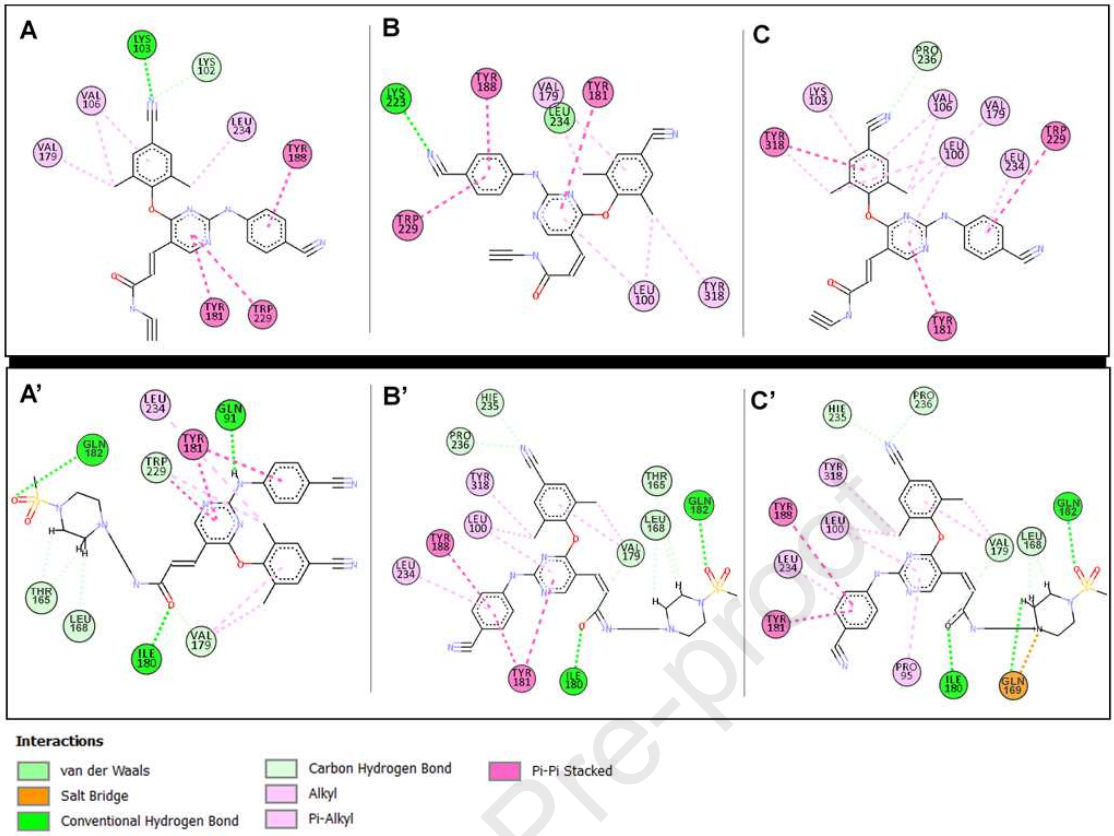

Figure 8. Analyses of complementary interactions differentially mediated by **14c** and **17l** at the NNIBP region. Occurring interactions due to extension of the **17l** methyl-sulphonyl piperazine group was also revealed.

1. A series of “dual-site” binding diarylpyrimidine derivatives were discovered.
2. Trans-double bond with spatial orientation advantage was introduced.
3. **14c** turned out to be potent inhibitor against single mutation strain E138K.
4. **14c** acted as classical NNRT inhibitors with high affinity for WT HIV-1 RT.
5. **14c** and **17l** are proposed as promising inhibitors by MD simulation.

Declaration of interests

☒ The authors declare that they have no known competing financial interests or personal relationships that could have appeared to influence the work reported in this paper.

☐The authors declare the following financial interests/personal relationships which may be considered as potential competing interests: